PLOS ONE

RESEARCH ARTICLE

Phytophthora infestans RXLR-WY Effector AVR3a Associates with Dynamin-Related Protein 2 Required for Endocytosis of the Plant Pattern Recognition Receptor FLS2

Angela Chaparro-Garcia, Simon Schwizer[¤a¤b], Jan Sklenar, Kentaro Yoshida[¤c], Benjamin Petre, Jorunn I. B. Bos[¤d], Sebastian Schornack[¤e], Alexandra M. E. Jones[¤f], Tolga O. Bozkurt[¤g]*, Sophien Kamoun*

The Sainsbury Laboratory, Norwich Research Park, Norwich, United Kingdom

¤a Current address: Boyce Thompson Institute for Plant Research, Ithaca, New York, United States of America.
¤b Current address: Department of Plant Pathology and Plant-Microbe Biology, Cornell University, Ithaca, New York, United States of America.
¤c Current address: Graduate School of Agricultural Science, Kobe University, Nada-ku, Kobe, 657–8501, Japan.
¤d Current address: Cell and Molecular Sciences, and Dundee Effector Consortium, James Hutton Institute, Invergowrie, Dundee, United Kingdom.
¤e Current address: Sainsbury Laboratory, University of Cambridge, Cambridge CB2 1LR, UK.
¤f Current address: School of Life Sciences, University of Warwick, Coventry, United Kingdom.
¤g Current address: Department of Life Sciences, Imperial College London, London, United Kingdom.
* o.bozkurt@imperial.ac.uk (TOB); sophien.kamoun@tsl.ac.uk (SK)

Citation: Chaparro-Garcia A, Schwizer S, Sklenar J, Yoshida K, Petre B, Bos JIB, et al. (2015) *Phytophthora infestans* RXLR-WY Effector AVR3a Associates with Dynamin-Related Protein 2 Required for Endocytosis of the Plant Pattern Recognition Receptor FLS2. PLoS ONE 10(9): e0137071. doi:10.1371/journal.pone.0137071

Editor: Boris Alexander Vinatzer, Virginia Tech, UNITED STATES

Received: February 5, 2015

Accepted: August 12, 2015

Published: September 8, 2015

Data Availability Statement: All relevant data are within the paper and its Supporting Information files.

Funding: This work was funded through grants by the Gatsby Charitable Foundation, European Research Council (ERC) and Biotechnology and Biological Sciences Research Council (BBSRC) to SK. The funders had no role in study design, data collection and analysis, decision to publish, or preparation of the manuscript.

Abstract

Pathogens utilize effectors to suppress basal plant defense known as PTI (Pathogen-associated molecular pattern-triggered immunity). However, our knowledge of PTI suppression by filamentous plant pathogens, i.e. fungi and oomycetes, remains fragmentary. Previous work revealed that the co-receptor BAK1/SERK3 contributes to basal immunity against the potato pathogen *Phytophthora infestans*. Moreover BAK1/SERK3 is required for the cell death induced by *P. infestans* elicitin INF1, a protein with characteristics of PAMPs. The *P. infestans* host-translocated RXLR-WY effector AVR3a is known to supress INF1-mediated cell death by binding the plant E3 ligase CMPG1. In contrast, AVR3a$^{KI\text{-}Y147del}$, a deletion mutant of the C-terminal tyrosine of AVR3a, fails to bind CMPG1 and does not suppress INF1-mediated cell death. Here, we studied the extent to which AVR3a and its variants perturb additional BAK1/SERK3-dependent PTI responses in *N. benthamiana* using the elicitor/receptor pair flg22/FLS2 as a model. We found that all tested variants of AVR3a suppress defense responses triggered by flg22 and reduce internalization of activated FLS2. Moreover, we discovered that AVR3a associates with the Dynamin-Related Protein 2 (DRP2), a plant GTPase implicated in receptor-mediated endocytosis. Interestingly, silencing of DRP2 impaired ligand-induced FLS2 internalization but did not affect internalization of the growth receptor BRI1. Our results suggest that AVR3a associates with a key cellular trafficking and membrane-remodeling complex involved in immune

Competing Interests: The authors have declared that no competing interests exist.

receptor-mediated endocytosis. We conclude that AVR3a is a multifunctional effector that can suppress BAK1/SERK3-mediated immunity through at least two different pathways.

Introduction

Plants must respond in a timely and effective manner to external cues such as biotic and abiotic stimuli. In particular, plants associate with a huge variety of microorganisms, many of which are sophisticated parasites [1–3]. To keep such parasitic microbes at bay, plants have evolved a multilayered immune system, which is triggered by microbial perception by receptors located at the cell surface and in the cytoplasm [3,4]. An important layer of defense relies on perception of pathogen associated molecular patterns (PAMPs) by cell surface localized pattern recognition receptors (PRRs), which triggers a basal defense response known as PAMP/PRR–triggered immunity (PTI) [5]. Early PTI signaling events include ion fluxes, reactive oxygen species (ROS) production, induction of mitogen-activated protein kinases (MAPKs) and calcium-dependent protein kinases (CDPKs), and transcriptional reprogramming [6–8]. Collectively, PTI contributes to immunity by delaying or arresting pathogen invasion, and in many cases PTI-deficient plant mutants become more susceptible to pathogens [9]. However, a common feature of adapted plant pathogens is the deployment of effector proteins that interfere with different steps in PTI signaling pathways [3,4,10,11]. This is particularly striking for bacterial plant pathogens, which evolved a battery of effectors to counteract PTI [3,12,13]. In contrast, our understanding of how eukaryotic pathogens, such as oomycetes and fungi, suppress PTI remains fragmentary [14–17].

The molecular signaling mechanisms activated after PAMP perception have been described for few PRRs. In *Arabidopsis thaliana* the leucine-rich repeat receptor-like kinases (LRR-RLKs) FLAGELLIN-SENSING 2 (FLS2) and EF-Tu RECEPTOR (EFR) recognize peptides derived from bacterial flagellin and elongation factor-Tu (EF-Tu), respectively [18]. In addition, the CHITIN ELICITOR RECEPTOR KINASE 1 (CERK1) and the LYSIN-MOTIF RECEPTOR-LIKE KINASE 5 (LYK5), together mediate binding and recognition of fungal chitin [19–24]. Activation of EFR and FLS2 leads to the recruitment of the regulatory LRR-RLK BRASSINOSTEROID INSENSITIVE 1 (BRI1)-associated receptor kinase (BAK1, also called SERK3) to activate signal transduction [25–29]. Interestingly, BAK1/SERK3 interacts with the RLK BRI1 (BRASSINOSTEROID INSENSITIVE 1) to regulate brassinosteroid signaling and plant growth [30–32], suggesting common regulatory mechanisms between plant growth and immunity [33].

In addition to LRR-RLKs, BAK1/SERK3 is also required for defense responses mediated by receptor like proteins (RLPs) [34,35]. More recently, BAK1/SERK3 emerged as a key component of basal defense against oomycetes, an important group of filamentous eukaryotic pathogens. Silencing of BAK1/SERK3 results in dramatically enhanced susceptibility and faster host colonization by the potato late blight pathogen *Phytophthora infestans* [36]. In addition, BAK1/SERK3 and its closest homolog BKK1/SERK4 are involved in resistance to the obligate biotrophic oomycete *Hyaloperonospora arabidopsidis* [28], providing further evidence of the role of BAK1/SERK3-dependent basal resistance against oomycete pathogens. BAK1/SERK3 contribution to basal defense against oomycetes is most likely the result of recognition of PAMPs [26,36,37]. Indeed, BAK1/SERK3 is required for the cell death response triggered by INF1, a secreted *P. infestans* protein with features of PAMPs [26,36].

Plant endocytic trafficking has emerged as a dynamic process that is diverted towards sites of pathogen infection [38,39] indicating that this process may play a critical role in immune responses [40]. FLS2 undergoes constitutive endocytosis and recycles between plasma

membrane and trans-Golgi network in a BAK1-independent manner to maintain steady-state levels at the cell surface [25,41]. In addition, FLS2 undergoes ligand-induced re-localization to endosomal vesicles in a BAK1-dependent manner [41–44]. Therefore, FLS2 traffics through two different endocytic pathways depending on its activation status. Furthermore, BRI1 and BAK1/SERK3 also undergo constitutive recycling via endosomes and can localize to overlapping endosomal compartments [32]. Receptor-mediated endocytosis was initially thought as a mechanism for attenuation of signaling through depletion of activated receptor complexes. Further studies in animal systems revealed that receptor internalization contributes to additional signaling at endocytic compartments [45]. In animal cells, late endosomal compartments, which contain internalized receptors, regulate signaling events such as pro-inflammatory signaling, growth, and development [45–49]. In plants, localization of BRI1 and BAK1/SERK3 as well as a brassinosteroid analog at the same endosomal compartments pointed to a possible link between internalization and signaling in growth regulation [32,50,51]. Nonetheless, defense-related endocytic signaling has yet to be unambiguously demonstrated in plants.

Mechanisms of receptor-mediated endocytosis involve clathrin-mediated and clathrin-independent pathways, resulting in the recruitment of a plasma membrane cargo [52–54] that is later invaginated and pinched off into the cytoplasm often by the action of the large GTPase dynamin [53,55]. Dynamin is a ~100 kDa protein that self-assembles into rings and helices to promote structural reorganization to mediate membrane fission [55]. The mechanistic details of clathrin-mediated endocytosis have been well established in animal cells and dynamin has been implicated in the internalization of the immunity-related Interleukin-2 Receptor (IL-2R) [56]. However, in plants, mechanisms of endocytosis have not been explicitly studied [57,58] and the extent to which dynamin or dynamin-like proteins play a role in receptor mediated endocytosis or plant immunity remains poorly understood.

P. infestans is the causal agent of potato and tomato late blight and a major threat to food security [59]. This oomycete pathogen deploys a large set of effectors that target multiple host cellular sites. Cytoplasmic effectors include the RXLR class, whose members are modular proteins that translocate inside host cells [60]. The biochemical activity of RXLR effectors is carried out by their C-terminal domains, which often contain variations of the conserved WY-domain fold [61,62]. One example of RXLR-WY effector is AVR3a of *P. infestans*. In *P. infestans* populations, *Avr3a* has two major allelic variants encoding the proteins AVR3a^{KI} and AVR3a^{EM}, which differ in two amino acids in the mature protein and are differentially recognized by the potato immune receptor R3a [63–68]. Contrary to AVR3a^{EM}, AVR3a^{KI} induces R3a-mediated resistance and confers avirulence to homozygous or heterozygous strains of the pathogen [63]. In host plants that do not carry R3a, AVR3a^{KI} effectively suppresses the cell death induced by *P. infestans* INF1 elicitin and is thought to contribute to pathogen virulence through this and other immune suppression activities [64,65,69]. Remarkably, AVR3a$^{KI\text{-}Y147del}$, a mutant with a deleted C-terminal tyrosine residue, is not affected in activation of R3a but fails to suppress INF1-mediated cell death, demonstrating that distinct amino acids condition the two AVR3a activities [65]. Moreover, AVR3a$^{KI\text{-}Y147del}$ neither binds nor stabilizes the plant E3 ubiquitin ligase protein CMPG1, which is required for INF1-mediated cell death, further uncoupling the effector activities [65,67]. The current model is that AVR3a, but not AVR3a-$^{KI\text{-}Y147del}$, binds and stabilizes CMPG1 to suppress BAK1/SERK3-regulated immunity triggered by INF1 during the biotrophic phase of *P. infestans* infection [67].

The current study was prompted by our discovery that natural variants of the *P. infestans* effector AVR3a (AVR3a^{KI} and AVR3a^{EM}) and the AVR3a$^{KI\text{-}Y147del}$ mutant suppress FLS2-dependent early responses. This contrasts sharply with the differential activities of these three AVR3a variants in suppressing INF1-mediated cell death, another BAK1/SERK3-dependent pathway. The ability of the AVR3a$^{KI\text{-}Y147del}$ mutant to suppress FLS2-dependent responses

revealed that AVR3a can suppress BAK1/SERK3-dependent responses in a CMPG1-independent manner. Furthermore, AVR3a reduced the internalization of the activated FLS2 receptor but did not interfere with its non-activated plasma membrane localization, indicating that this effector might target cellular trafficking initiated at the cell periphery. Consistent with this model, we found that AVR3a associates with a plant GTPase dynamin-related protein 2 (DRP2) involved in receptor-mediated endocytosis, implicating AVR3a in a cellular trafficking complex. Furthermore, we found that DRP2 is required for internalization of FLS2 and that overexpression of DRP2 suppressed PRR-dependent accumulation of reactive oxygen species (ROS). We conclude that AVR3a associates with a key cellular trafficking and membrane-remodeling complex that may be required for PRR endocytic trafficking.

Results

AVR3a suppresses PTI in a CMPG1-independent manner

To determine the degree to which AVR3a suppresses PAMP-elicited defense responses besides INF1-mediated cell death, we measured reactive oxygen species (ROS) production and defense gene induction in *N. benthamiana* triggered by bacterial and oomycete elicitors. Plants transiently expressing epitope tagged variants of AVR3a (FLAG-AVR3a^{KI}, FLAG-AVR3a^{EM}, FLAG-AVR3a$^{KI\text{-}Y147del}$) or a vector control (pBinplus::ΔGFP) were treated with flg22 (100 nM) or INF1 (10 μg/ml) and the transient accumulation of reactive oxygen species (ROS) was followed over 45 minutes or 22 hours, respectively. We observed that all variants of AVR3a reproducibly suppressed flg22-induced ROS accumulation to the same extent whereas AVR3a^{KI} suppressed INF1-induced ROS accumulation more effectively than the other two variants, which is consistent with previous reports [64,65] (Fig 1A and 1C). We obtained similar results after flg22 treatment in *N. benthamiana* and *A. thaliana* plants stably expressing AVR3a, validating the transient expression assays (Panel A and B in S1 Fig).

The immune responses triggered by another bacterial PAMP, EF-Tu, overlap and share signaling components with those triggered by flagellin [28,70,71]. Therefore, we tested the effect of AVR3a on ROS accumulation triggered by the EF-Tu derived peptide elf18. We found that elf18 ROS production was significantly impaired to a similar extent by all variants of AVR3a (Panel A in S2 Fig). In contrast, the BAK1/SERK3-independent ROS production in response to chitin was not affected by any of the AVR3a variants (Panel B in S2 Fig). These results may indicate that AVR3a suppresses BAK1/SERK3-dependent pathways but not BAK1-independent immune responses.

One of the outcomes of PAMP elicitation is transcriptional reprogramming, a defense response occurring downstream of ROS production [9]. Therefore, we monitored the effect of AVR3a on gene expression of the previously characterized PTI marker genes *NbCYP71D20* and *NbACRE31* [26,72]. *NbCYP71D20* expression was induced ~12-fold by flg22 and ~80-fold by INF1 treatment in control plants (Fig 1B and 1D). All AVR3a variants reduced the induction of *NbCYP71D20* by flg22 by approximately 80% (Fig 1B) whereas reduction of INF1-elicited gene induction was about 40% for AVR3a^{KI} and AVR3a^{EM} with no reduction observed for the AVR3a$^{KI\text{-}Y147del}$ variant (Fig 1D). Similarly, induction of *NbACRE31* by flg22 treatment decreased by 80% in the presence of all variants of AVR3a (Panel C in S1 Fig). In contrast, AVR3a did not suppress *NbACRE31* expression after INF1 elicitation, although INF1 induction of this gene was very low (Panel D in S1 Fig).

Overall, our results indicate that in addition to suppressing INF1-mediated cell death [64,65,67], AVR3a has the capacity of supressing PTI responses mediated by the BAK1/SERK3-dependent cell surface receptors FLS2 and EFR. Remarkably, all the variants of AVR3a, including AVR3a$^{KI\text{-}Y147del}$, which neither suppresses INF1-mediated cell death nor interacts

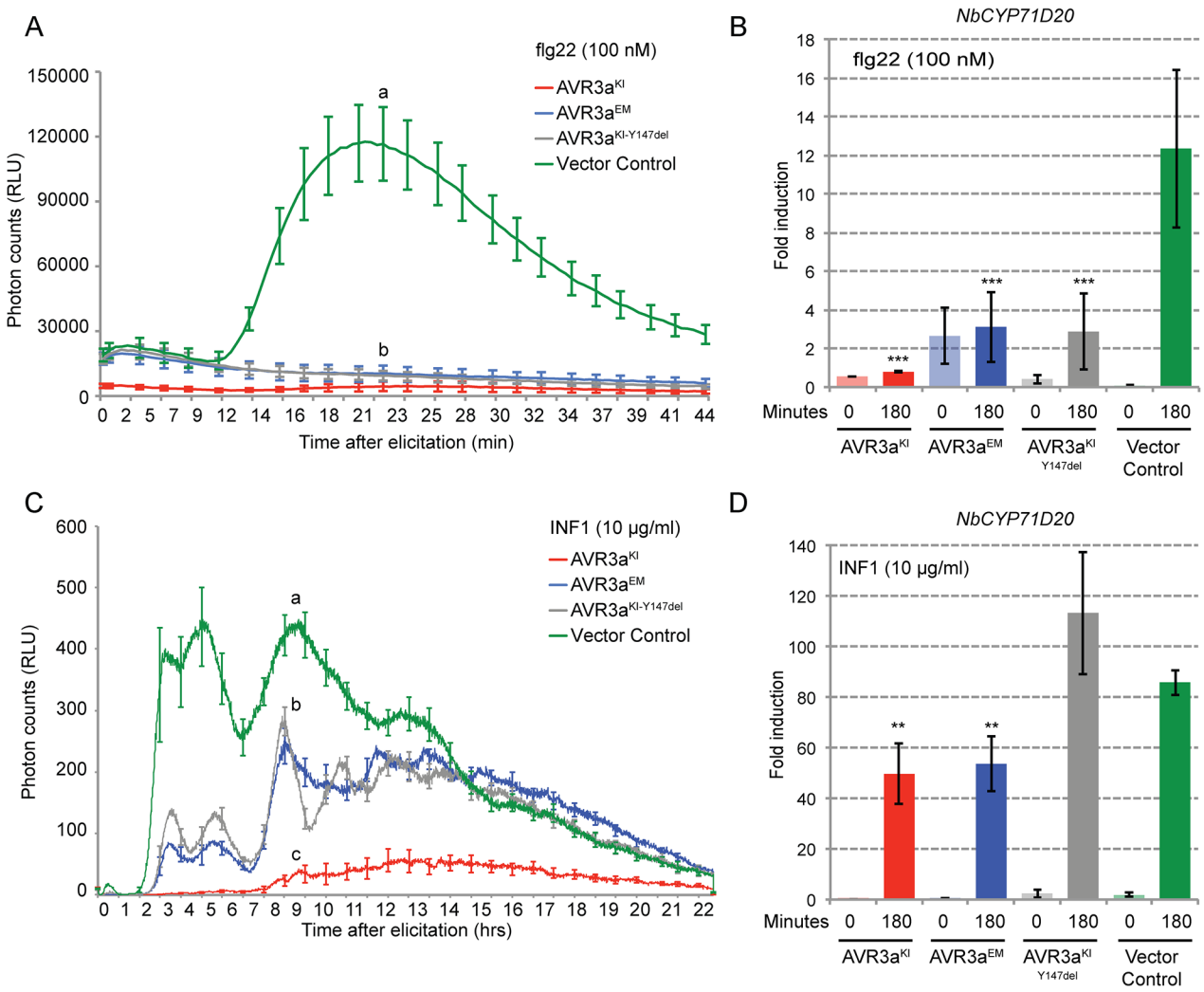

Fig 1. AVR3a suppresses elicitor-induced reactive oxygen species (ROS) production and gene expression induction. (A, C) Time course experiments measuring ROS production in relative light units (RLU) in response to 100 nM flg22 (A) or 10 µg/ml INF1[Pi] (C) in *N. benthamiana* transiently expressing FLAG-AVR3a^{KI} (red), FLAG-AVR3a^{EM} (blue), FLAG-AVR3a$^{KI\text{-}Y147del}$ (grey) or Vector Control (ΔGFP, green). Different letters above the graph indicate significant differences at $P < 0.001$ assessed by one-way ANOVA followed by TukeyHSD test. (B, D) Quantitative RT-PCR analysis of expression of the marker gene *NbCYP71D20* by 100 nM flg22 (B) or 10 µg/ml INF1[Pi] (D) in *N. benthamiana* stably expressing the same FLAG-AVR3a constructs. Marker gene expression was assessed at time 0 and 180 minutes after elicitor treatment and transcript levels were normalized to the *NbEF1α* housekeeping gene. Results are average SE (n = 3 technical replicates). Statistical significance was assessed by one-way ANOVA followed by TukeyHSD test. $^{**}P < 0.01$; $^{***}P < 0.001$. Similar results were observed in at least three independent experiments.

doi:10.1371/journal.pone.0137071.g001

with the E3 ligase CMPG1, suppressed flg22 responses to the same extent. These findings indicate that the newly identified suppression activity is CMPG1-independent and that the AVR3a effector may suppress PTI through multiple mechanisms.

AVR3a does not alter receptor levels at the cell surface or receptor complex formation

The bacterial effector AvrPtoB targets FLS2 for degradation to suppress plant immunity [73]. This prompted us to determine whether the suppression of flg22-triggered responses by AVR3a involved perturbation of FLS2 or BAK1 protein accumulation or complex formation [74,75]. To address this question, we transiently co-expressed AVR3a variants with FLS2-GFP

or BAK1/SERK3-YFP in *N. benthamiana* and assessed the fusion protein levels. We found that AVR3a did not alter FLS2 or BAK1/SERK3 protein accumulation *in planta* (Fig 2A). Next, we tested whether AVR3a^{KI} perturbed heterodimerization of FLS2 with BAK1/SERK3 after flg22 treatment [25,26,28]. We used leaves of transgenic *N. benthamiana* plants stably expressing AVR3a^{KI} or a vector control and transiently expressed FLS2-GFP and BAK1/SERK3-HA. In the presence of AVR3a^{KI} a double band signal appeared (WB:HA) for BAK1/SERK3 total protein extracts (Fig 2B) that was not seen after immunoprecipitation. However, this observation was not consistent between experiments and probably is the result of protein degradation during protein extraction. After co-immunoprecipitation, AVR3a did not prevent the flg22-triggered association between FLS2 and BAK1/SERK3 (Fig 2B). In summary, these results suggest that AVR3a does not interfere with receptor protein accumulation or complex formation and that the effector suppression of flg22 responses most likely occurs downstream of FLS2/BAK1 heterodimerization.

AVR3a interferes with FLS2 internalization

We hypothesized that AVR3a alters the subcellular distribution of FLS2 and/or BAK1/SERK3 to perturb their activities. To determine the effect of AVR3a on subcellular distribution of the receptors, we transiently co-expressed FLS2-GFP or BAK1/SERK3-YFP with AVR3a variants in *N. benthamiana* and assessed the localization of the non-activated receptors by confocal microscopy. In both cases, AVR3a did not alter the previously reported plasma membrane localization of FLS2 and BAK1/SERK3 [31,42] (Fig 3A). We then examined whether AVR3a has an effect in the non-activated subcellular localization of other cell surface receptors. We co-expressed EFR and CERK1 with all AVR3a variants in *N. benthamiana* and found that AVR3a did not alter the membrane localization of these immune receptors (S3 Fig).

FLS2 activation after flg22 perception leads to endocytosis and accumulation of the receptor in mobile endosomal compartments [41,42,44]. To test whether AVR3a has an effect on the subcellular distribution of an activated receptor, we transiently expressed FLS2-GFP in *N. benthamiana* plants expressing a vector control. We detected FLS2-GFP vesicles at 80 minutes to 150 minutes after flg22 elicitation (Fig 3B and S4 Fig), whereas we rarely detected vesicle-like structures in cells treated with water (Fig 3B). Remarkably, the flg22-induced FLS2 endosomal localization was partially inhibited in plants expressing AVR3a (AVR3a^{KI} or AVR3a^{EM} or AVR3a$^{KI\text{-}Y147del}$) (Fig 3B and S4 Fig). To evaluate the robustness of this phenomenon, we quantified the number of flg22-induced FLS2-GFP endosomes, seen as distinct fluorescent signal in punctate structures. We found that in the presence of AVR3a (AVR3a^{KI} or AVR3a^{EM} or AVR3a$^{KI\text{-}Y147del}$), the number of FLS2-GFP labelled endosomes was reduced down to almost half compared to the control (Fig 3B and 3C). Thus, we conclude that AVR3a partially inhibits FLS2 internalization.

Next, we assessed whether AVR3a specifically inhibits the internalization of FLS2 or if it generally interferes with endocytic processes. For this we used BRI1, a receptor involved in development that also requires BAK1/SERK3 for its activity and shows constitutive internalization [32]. Using the same experimental procedure described above, we observed that BRI1-GFP fluorescent signal from vesicle-like structures was unaltered in the presence of AVR3a^{KI} (Panel A and B in S5 Fig). These results suggest that AVR3a interferes with FLS2 internalization without affecting general receptor endocytosis, possibly by targeting a plant protein specifically required for FLS2 internalization.

AVR3a associates with DRP2, a plant protein involved in cellular trafficking

AVR3a was previously shown to bind the E3 ligase CMPG1 [67]. To determine which additional host proteins associate with AVR3a, we used immunoprecipitation of FLAG-AVR3a^{KI}

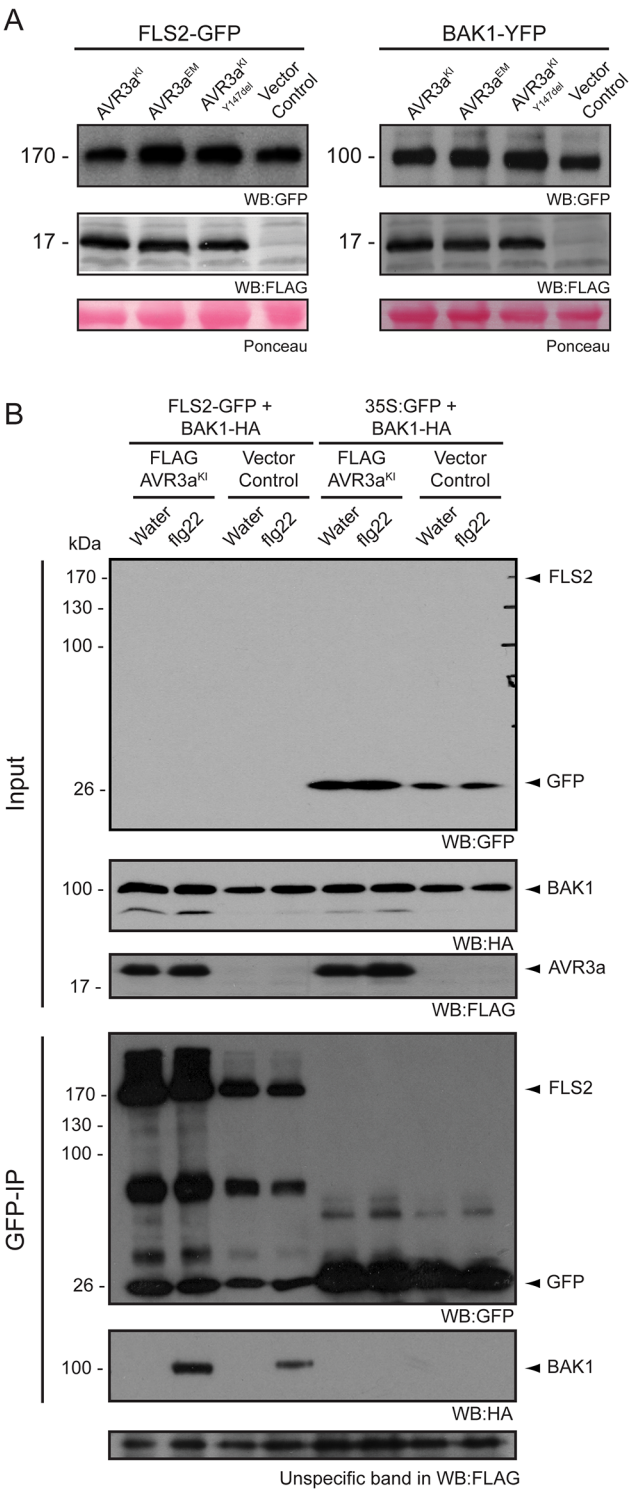

Fig 2. AVR3a does not affect protein accumulation of the non-activated receptors FLS2 and BAK1 or their association *in planta*. (A) Transient co-expression in *N*. *benthamiana* of FLS2-GFP or BAK1-YFP with FLAG-AVR3a^{KI} or FLAG-AVR3a^{EM} or FLAG-AVR3a$^{KI\text{-}Y147del}$ or Vector Control (ΔGFP) as indicated. Total proteins were isolated at 2.5 days post infiltration (dpi) and total extracts were subjected to immunoprecipitation with 8 μl of anti-GFP agarose beads (Chromotek) to enrich for the GFP-tagged proteins, and detected using anti-GFP antibody. Equal amounts of protein were analyzed (Ponceau lane) in all cases. (B) Transgenic *N*. *benthamiana* expressing FLAG-AVR3a^{KI} or vector control (ΔGFP) were transiently infiltrated with a mix (1:1) of

FLS2-GFP/BAK1-HA and treated with flg22 (100 nM) or water for 15 minutes. Treated leaf-tissues were collected at 2.5 dpi and subjected to co-immunoprecipitation with 25 μl GFP agarose beads (Chromotek). Purified complex formation after flg22 treatment of FLS2-GFP and BAK1-HA was analyzed by immunoblotting with the specified antibodies. 35S:GFP/BAK1-HA was used as a control. Note that FLS2-GFP was almost never detected in the total extracts (Input) but became visible by western blot analysis after immunoprecipitation.

doi:10.1371/journal.pone.0137071.g002

expressed in *N. benthamiana* followed by liquid chromatography-tandem mass spectrometry (LC-MS/MS) analysis using previously described methods [76]. We identified four proteins that associated with AVR3a^{KI} that had unique peptide counts compared to the controls in two biological replicates (S1 Table). We selected a homolog of the GTPase dynamin-related protein (DRP) (NCBE_074039.1) for further investigation based on the established role of dynamins in cellular trafficking and clathrin-mediated endocytosis in animal systems [77]. In mammals, dynamin is a five-domain protein consisting of a GTPase domain, an unstructured middle domain, a Pleckstrin-homology domain, a GTPase effector (GED) domain and a proline-rich domain, and its functions range from vesicle scission during endocytosis to the formation of the tubular-vesicular network during cytokinesis [77]. In Arabidopsis, DRP2A and DRP2B (previously known as ADL6 and ADL3, respectively) are the only dynamin-related proteins (DRP) with a domain architecture similar to other canonical dynamins [77–80]. Database searches using the tblastn algorithm and NCBE_074039.1 as the protein query sequence revealed that DRP2A and DRP2B are the most similar proteins for NCBE_074039.1. Therefore, we designed primers based on the Arabidopsis DRP2A and DRP2B sequences and the partial *N. benthamiana* sequences available at the time of the experiment. However, PCR reactions using these primers and *N. benthamiana* leaf cDNA as a matrix did not produce amplicons. As an alternative strategy, we cloned two putative DRP2 proteins from *Nicotiana tabacum*, termed NtDRP2–1 and NtDRP2–2, which share 99% amino acid sequence identity. Sequence analysis revealed that NtDRP2–1 and NtDRP2–2 have the classical five-domain structure of canonical dynamin proteins [77] and have 77% amino acid sequence similarity to the Arabidopsis DRP2 proteins (S6 Fig). To determine the evolutionary relationship of NtDRP2–1/2 to other plant DRPs, we first searched the genomes of solanaceous species, Arabidopsis and other dicot plants for proteins containing the dynamin signature [81]. Next, we constructed a maximum likelihood tree based on the amino acid sequence alignment of the conserved GTPase-domain of 45 identified DRPs (S7 Fig and S2 Table). The tree confirmed that NtDRP2–1/2 are most similar to AtDRP2A and AtDRP2B among the 11 Arabidopsis DRPs (S7 Fig).

We then investigated the subcellular localization of NtDRP2 to determine whether it is consistent with the presumed function of DRPs in cellular trafficking. Transient expression of GFP-NtDRP2–1 and GFP-NtDRP2–2 in *N. benthamiana* followed by confocal microscopy revealed that GFP-NtDRP2–1 and GFP-NtDRP2–2 mainly localized to the plasma membrane, as confirmed by the formation of thin cytoplasmic strands at points of adhesion between the plasma membrane and the cell wall (Hechtian strands) after plasmolysis treatment (Panel B and C in S8 Fig). In addition, GFP-NtDRP2–1 and GFP-NtDRP2–2 localized to the cytosol in a punctate pattern (Panel C in S8 Fig). This subcellular distribution is consistent with the reported localization of canonical dynamins in animal, yeast and Arabidopsis [77,78,82,83].

Next we validated the association of AVR3a with the cloned NtDRP2–1 *in planta* by co-immunoprecipitation analysis. All three AVR3a variants co-immunoprecipitated with GFP-NtDRP2–1 when expressed in *N. benthamiana* as FLAG epitope tagged proteins (Fig 4). The RXLR effector AVRblb2 was used as a negative control in these experiments as it failed to co-immunoprecipitate with NtDRP2–1 (Fig 4). We also used the *Phytophthora capsici* effector PcAVR3a-4 [61] as an additional negative control because this AVR3a homolog does not

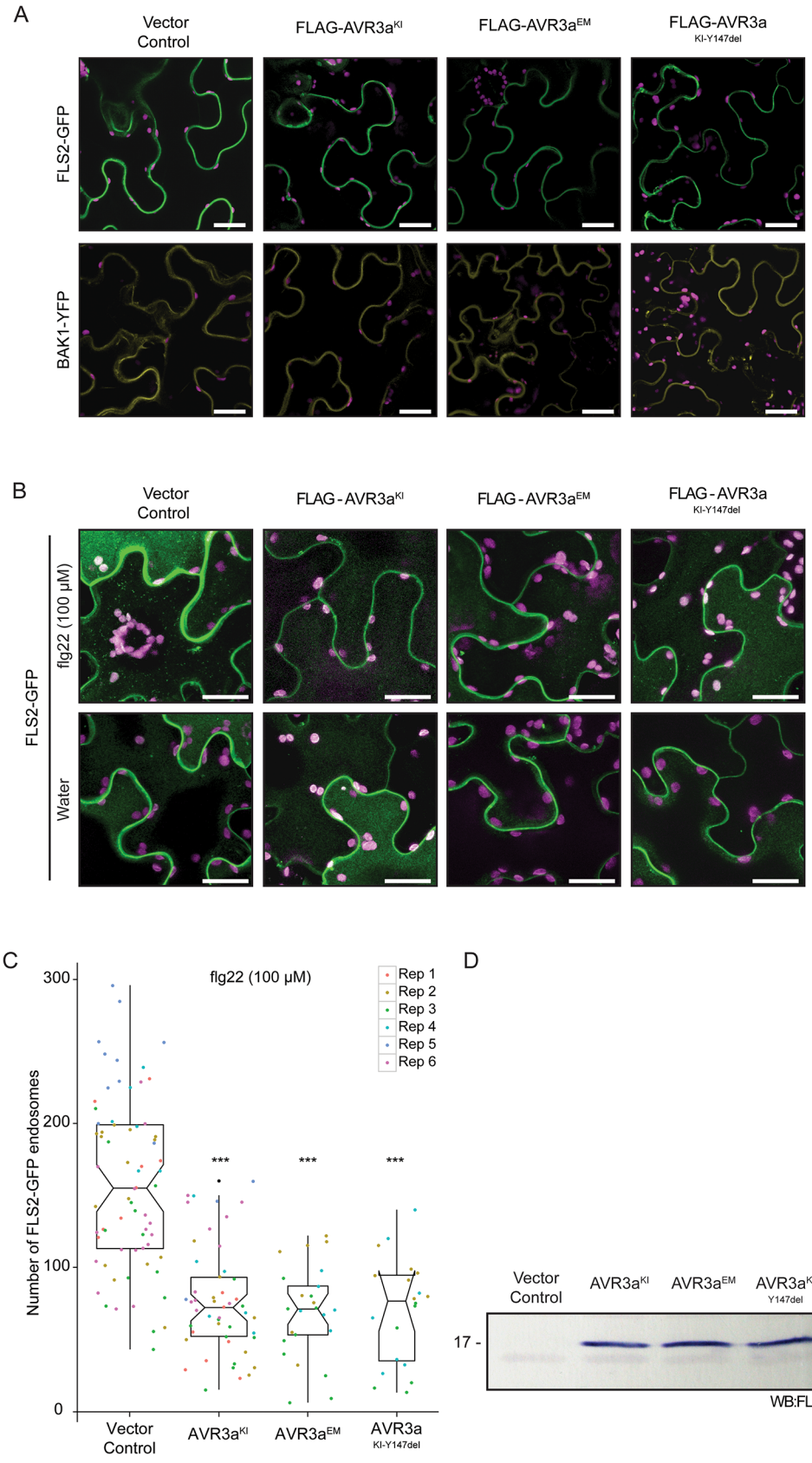
A
Vector Control
FLAG-AVR3a^KI
FLAG-AVR3a^EM
FLAG-AVR3a KI-Y147del
FLS2-GFP
BAK1-YFP
B
Vector Control
FLAG - AVR3a^KI
FLAG - AVR3a^EM
FLAG - AVR3a KI-Y147del
FLS2-GFP
flg22 (100 µM)
Water
C
flg22 (100 µM)
Rep 1
Rep 2
Rep 3
Rep 4
Rep 5
Rep 6
Number of FLS2-GFP endosomes
300
200
100
0
***
***
***
Vector Control
AVR3a^KI
AVR3a^EM
AVR3a KI-Y147del
D
Vector Control
AVR3a^KI
AVR3a^EM
AVR3a^KI Y147del
17 -
WB:FLAG

Fig 3. AVR3a partially suppresses the endosomal localization of the activated FLS2 receptor. (A) Confocal microscopy in *N. benthamiana* leaf pavement cells stably expressing FLAG-AVR3a^{KI}, FLAG-AVR3a^{EM}, FLAG-AVR3a$^{KI\text{-}Y147del}$ or vector control (ΔGFP) and infiltrated with FLS2-GFP or BAK1-YFP. The effector AVR3a did not alter the non-activated FLS2 (green) or BAK1 (yellow) plasma membrane subcellular localization at 2.5 days post infiltration (dpi). Scale bar = 25 μm. Plastid auto-fluorescence (purple) is shown. (B) Standard confocal images of FLS2-GFP in *N. benthamiana* leaf pavement cells under the same conditions described above, challenged for 90 to 120 minutes with 100 μM flg22 or water as indicated. Representative images show a clear accumulation of FLS2-GFP in intracellular vesicles (green dots) specifically after flg22 elicitation in the vector control plants whereas this distinct re-distribution of FLS2-GFP was partially inhibited by the presence of all variants of AVR3a. All images are a maximum projection of 20 optical sections taken at 1-μm intervals. Same confocal settings were used to acquire all images. Scale bar = 25 μm. Plastids auto-fluorescence (purple) is shown. (C) Quantification of the effect of AVR3a on FLS2 endocytosis. Scatter plots show the number of FLS2-GFP endosomes per total image area in the presence of flg22 from 6 independent biological experiments. Vector control (ΔGFP) n = 69, FLAG-AVR3a^{KI} n = 49, FLAG-AVR3a^{EM} n = 25, FLAG-AVR3a$^{KI\text{-}Y147del}$ n = 20. Statistical significance was assessed by Wilcoxon-Mann-Whitney Test. ***$P < 0.001$. (D) Western blot probed with anti-FLAG antibody showing the expression of AVR3a in transgenic *N. benthamiana* plants.

doi:10.1371/journal.pone.0137071.g003

suppress the ROS burst induced by flg22 (Panel B in S9 Fig). Indeed, in side-by-side co-immunoprecipitation experiments we only detected a weak NtDRP2–1 band signal after increasing exposure times (Panel A in S9 Fig). Overall, these results confirm that all AVR3a variants associate with NtDRP2–1 and suggest this association may be linked to the ability of AVR3a to suppress responses elicited by flg22.

DRP2 dynamin is required for FLS2 internalization

In a recent independent study, Smith and colleagues [84] showed that DRP2B functions in flg22-signaling and bacterial immunity in Arabidopsis [84]. To further investigate the link between AVR3a activities and NtDRP2, and notably the degree to which DRP2 is required for FLS2 internalization, we used RNAi silencing experiments. We designed silencing constructs that target *N. benthamiana* DRP2 *Nb05397* (*NbDRP2–1*) and *Nb31648* (*NbDRP2–2*), which are the most similar proteins to NtDRP2–1 and NtDRP2–2 in *N. benthamiana* (S7 Fig). Reports in Arabidopsis showed that members of the DRP2 family are implicated in cell cytokinesis and post-Golgi vesicular trafficking, and are essential for development since *drp2* double mutants exhibit pleiotropic developmental defects [78–80,85]. Indeed, using virus-induced gene silencing (VIGS) in *N. benthamiana*, we observed that plants silenced for *NbDRP2–1* and *NbDRP2–2* display severe developmental defects and ultimately become necrotic and died confirming the essential role of dynamins in plant development (S10 Fig). To circumvent VIGS-induced lethality, we transiently expressed a *DRP2*-targeted hairpin-silencing construct in fully developed *N. benthamiana* leaves to silence *Nb05397* and *Nb31648* (Panel A in S11 Fig). Using quantitative RT-PCR, we confirmed that the hairpin construct reduced the mRNA levels of *Nb05397* and *Nb31648* but not of the two other related *N. benthamiana DRP2* genes *Nb11538* and *Nb09838*, indicating that the RNAi silencing is specific to the targeted *N. benthamiana DRP2* genes (Panel B in S11 Fig). We also confirmed that the silenced epidermal cells remained viable by staining with propidium iodide (Panel C in S11 Fig).

Next, we used the hairpin RNAi system to determine the effect of silencing *NbDRP2* in *N. benthamiana* leaves on flg22-induced internalization of FLS2-GFP. We found that FLS2-GFP containing vesicles were reduced in the *NbDRP2* silenced leaves upon flg22 treatment, but were clearly visible in control-silenced leaves (Fig 5A and 5C). Moreover, silencing *NbDRP2* did not alter accumulation of FLS2 at the plasma membrane in water treated samples (Fig 5A), indicating that DRP2 only affects FLS2 after activation. To determine whether the effect of *NbDRP2*-silencing on receptor internalization is specific to FLS2, we performed the same *NbDRP2* RNAi experiments with BRI1. Remarkably, BRI1-GFP constitutive endocytosis was not affected in

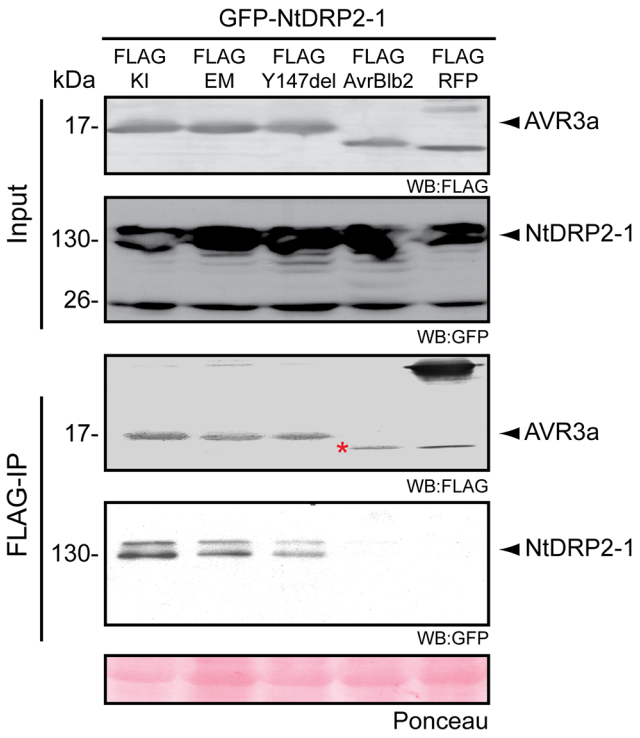

Fig 4. AVR3a associates with NtDRP2–1 *in planta*. GFP-NtDRP2–1 was transiently co-expressed with FLAG-AVR3a^{KI} or FLAG-AVR3a^{EM} or FLAG-AVR3a$^{KI\text{-}Y147del}$ or FLAG-AVRblb2 or vector control (FLAG-RFP) in *N. benthamiana*. Immunoprecipitates obtained with anti-FLAG beads (SIGMA) and total protein extracts were immunoblotted with the appropriate antisera. Proteins were isolated 2.5 days post infiltration. Red asterisk indicates FLAG-tagged AVRblb2 protein in the total extract. Experiment repeated at least three times with similar results.

doi:10.1371/journal.pone.0137071.g004

leaves silenced for *NbDRP2* and a similar number of BRI1-GFP labelled vesicles was observed in the *NbDRP2* RNAi treatment compared to the negative control (Panel C and E in S5 Fig). We conclude that *NbDRP2* is required for ligand-induced endocytosis of FLS2 and that this requirement might be specific for immune-related receptors. Importantly, these findings are consistent with our earlier finding that AVR3a interferes with the internalization of the activated FLS2 receptor but not BRI1 (Fig 3B and 3C, S4 and panel A and B in S5 Figs).

Overexpression of NtDRP2 dynamin suppresses flg22-induced ROS burst

To assess the role of Solanaceous DRP2 in early defense responses, we first determined the degree to which silencing of *NbDRP2* affects flg22-induced ROS production. Although we observed a reduction in flg22-induced ROS accumulation in *NbDRP2*-silenced *N. benthamiana* leaves, the effect was inconsistent and was only noted in 40% of the experiments (n = 10) (S12 Fig). We then determined the effect of overexpressing NtDRP2 in *N. benthamiana* on ROS production upon flg22 treatment. Consistent with the finding that AtDRP2B is a negative regulator of flg22-triggered ROS [84], we found that NtDRP2–1/2 decreased flg22-induced ROS burst by more than 50% compared to plants expressing a vector control (Fig 6A). In addition, NtDRP2–1 significantly reduced the ROS production in response to INF1 and chitin treatments (Fig 6B and 6C). These results might indicate that the effect of DRP2 on ROS responses

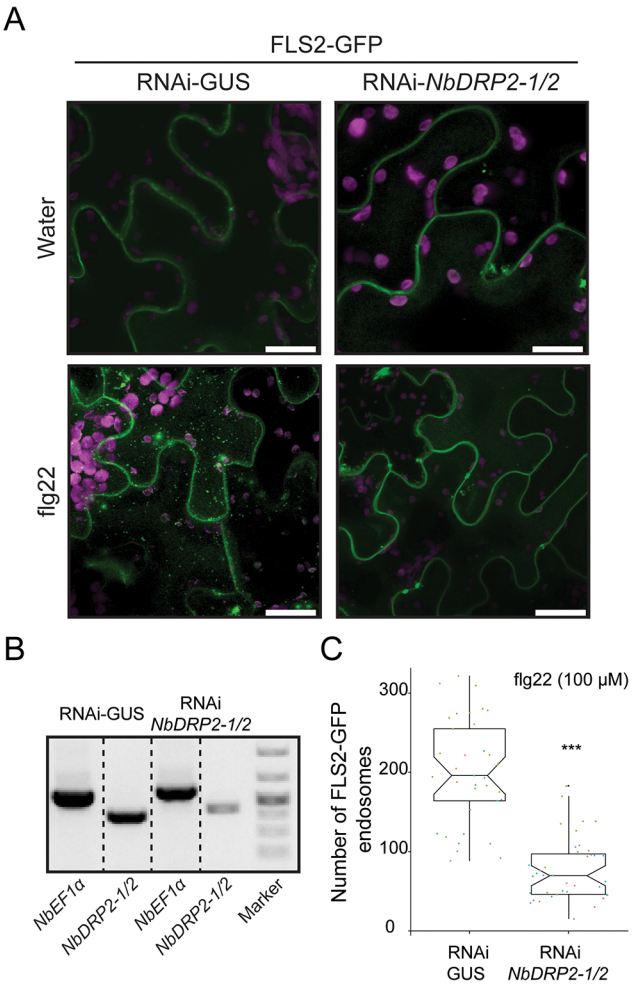

Fig 5. *NbDRP2–1/2* is required for FLS2 internalization. (A) Confocal imaging in *N. benthamiana* pavement cells reveals that decreased *NbDRP2–1/2* expression leads to a significant reduction of subcellular distribution of FLS2-GFP in endosomes (green dots) after flg22 elicitation (100 μM). *N. benthamiana* leaves were transiently expressing FLS2-GFP plus a hairpin-silencing construct RNAi-*NbDRP2–1/2* or the silencing vector control RNAi-GUS. Imaging was done at 2.5 days post infiltration. All images are a maximum projection of 21 optical sections taken at 1-μm intervals. Same confocal settings were used to acquire all images. Bar = 25 μm. Plastids auto-fluorescence (purple) is shown. (B) Validation of RNAi-*NbDRP2–1/2* silencing by RT-PCR in leaf-discs collected from the same leaves used for microscopy. Bands were grouped in the Fig and dashed black lines represent different parts of the same gel. (C) Quantification of the effect of RNAi-*NbDRP2–1/2* on FLS2 endocytosis. Scatter plots show the number of FLS2-GFP endosomes per total image area in the presence of flg22 from 5 independent biological experiments. RNAi-GUS n = 39, RNAi-*NbDRP2–1/2* n = 40. Statistical significance was assessed by Wilcoxon-Mann-Whitney Test. ***$P < 0.001$.

doi:10.1371/journal.pone.0137071.g005

is not limited to BAK/SERK3-dependent pathways potentially placing NtDRP2 as a modulator of early signaling responses induced by several PAMPs.

Discussion

Even though perception of pathogen-associated molecular patterns significantly contributes to basal defense of plants against *P. infestans*, our knowledge of how *P. infestans* effectors subvert PTI is patchy. One of the most studied effectors of *P. infestans* is the RXLR-WY type effector AVR3a [63–67,69,86]. In this study, we further characterized the virulence activities of AVR3a and discovered that AVR3a suppresses early defense responses mediated by the cell surface

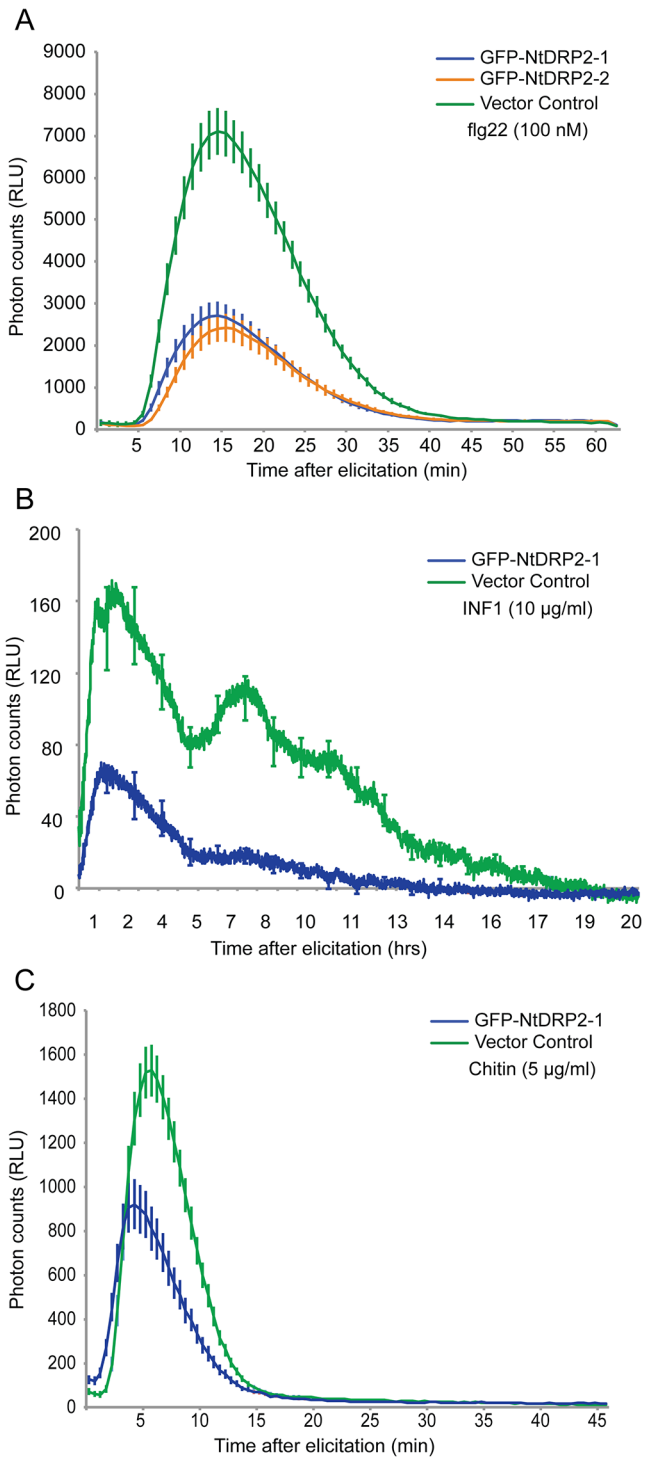

Fig 6. Overexpression of NtDRP2 reduces the accumulation of ROS upon PAMP perception. (A, B, C) *Agrobacterium tumefaciens*-mediated transient expression of GFP-NtDRP2–1 or vector control (35:GFP) in *N. benthamiana* leaves showed that ROS production after elicitation with flg22 (A), INF1 (B) or chitin (C) is reduced in the presence of NtDPR2. Total ROS production was measured in relative light units (RLU) over time after treatment with 100 nM flg22 (A), with 10 µg/ml INF1[Pi] (B) or with 5 µg/ml chitin (SIGMA) (C). ROS production was measured at 3 days post infiltration. Similar results were obtained in at least four independent experiments.

doi:10.1371/journal.pone.0137071.g006

immune co-receptor BAK1/SERK3, which contributes to basal immunity against *P. infestans* [36]. More specifically, we provide evidence that AVR3a reduces internalization of the activated pattern-recognition receptor FLS2 but neither interferes with the plasma membrane localization of non-activated FLS2 nor perturbs the steady state levels of this immune receptor or other PRRs. Furthermore, we found that AVR3a associates with DRP2, a *Solanaceae* member of the plant GTPase dynamin family whose members mediate endocytosis and membrane remodeling [87]. Interestingly, DRP2 is required for FLS2 internalization but does not affect internalization of the growth receptor BRI1.

Several bacterial type III secretion system effectors target cell surface immune receptor complexes to modulate their activities and suppress plant immunity [13,73,75]. AVR3a is an example of a filamentous plant pathogen effector that has evolved to deregulate plant immune signaling, including suppression of the cell death triggered by several pathogen molecules, among them the elicitin molecular pattern of oomycetes [64,67,69]. Our results further demonstrate that AVR3a contributes to suppression of basal defense responses similar to bacterial effectors. However, the exact molecular mechanisms by which eukaryotic effectors such as AVR3a subvert plant immunity remains poorly known. A recent screen showed the potential of *P. infestans* RXLR effectors to suppress early PTI signaling [88]. Although several RXLR effectors suppressed flg22-mediated PTI responses, AVR3a was not able to suppress the activation of the flg22-responsive *FRK1* gene in tomato or Arabidopsis protoplasts [88]. The difference with our results could be due to intrinsic experimental differences, since the reporter screen was performed on protoplasts and the mechanisms of PTI suppression may vary under those conditions. Alternatively, it may indicate a level of specificity for the AVR3a suppression activity. Indeed, here we showed that AVR3a equally suppresses the activation of two marker genes after flg22 treatment but differentially suppressed the same marker genes set upon INF1 elicitation (Fig 1 and S1 Fig). Nevertheless, our work is consistent with the previous finding that AVR3a blocks signal transduction cascades initiated at the plasma membrane after pathogen perception [69]. Importantly, we found that interference with FLS2 signaling and endocytosis does not involve the interaction with the E3 ligase CMPG1 since AVR3a$^{KI\text{-}Y147del}$, a variant that is unable to bind and stabilize CMPG1, is still able to suppress flg22-triggered ROS production and endocytosis (Fig 1A, Fig 3B and 3C). Therefore, AVR3a is a multifunctional effector that can suppress BAK1/SERK3-mediated immunity through at least two different pathways, possibly by acting at different sites or at different time points during immune signaling.

The step at which AVR3a interferes with FLS2 signaling is unclear. AVR3a did not alter subcellular localization of FLS2 or BAK1/SERK3 (Fig 3A and S3 Fig) and it did not affect ligand induced complex formation between FLS2 and BAK1/SERK3 (Fig 2). However, the receptor complex somehow remained inactive in the presence of AVR3a given that downstream signaling cascades were not activated. Given that elicitor-induced internalization of FLS2 occurs in a BAK1-dependent manner [42,43] it is possible that the effect of AVR3a in FLS2 internalization occurs via BAK1/SERK3. However, BAK1/SERK3 C-terminal fusions are partially impaired in early PTI responses [89], and assays evaluating the extent to which BAK1/SERK3 undergoes endocytosis after flg22 perception can be difficult to interpret. Interestingly, AVR3a exhibits some degree of specificity in suppressing PAMP-triggered immunity. Unlike the *P. syringae* effector AvrPtoB, which blocks the responses elicited by bacterial flagellin and chitin [90–92], none of the AVR3a variants suppressed chitin-induced ROS burst suggesting that AVR3a specifically suppresses BAK1/SERK3-dependent immune responses. At this stage, we propose that AVR3a interferes with BAK1/SERK3-mediated cellular trafficking involved in the perception of pathogens at the cell periphery but additional work is needed to clarify the underlying mechanisms.

Our finding that AVR3a co-immunoprecipitates with DRP2 does not necessarily imply that these two proteins directly bind *in-planta* nor that DRP2 is a target of the effector. DRP2 could be a helper (facilitator) of AVR3a that functions as a cofactor or enables localization of AVR3a to particular subcellular compartments as defined by Win et al. [4]. Whether AVR3a affects the biochemical activity or regulation of DRP2 remains to be studied. However, AVR3a is unlikely to completely inhibit DRP2 activity since DRP2 silencing resulted in plant lethality unlike transient or stable *in planta* expression of AVR3a. Nonetheless, our results place AVR3a in proximity to a membrane-remodeling complex that is implicated in endocytosis of the cell surface pattern-recognition receptor FLS2.

Although we cannot rule out that PTI suppression and inhibition of FLS2 endocytosis by AVR3a are two unrelated processes, AVR3a affected FLS2 but not BRI1 endocytosis, suggesting that AVR3a may specifically affect PRRs activities and that the mechanisms for FLS2 and BRI1 internalization may be different. Indeed, previous reports have shown that the regulatory role of BAK1/SERK3 in BR and PTI signaling are distinct and can be mechanistically uncoupled [71,89]. In addition, there are different pools of BAK1/SERK3 that are not interchangeable between BRI1 and FLS2 and activation by BR or flg22 does not cross activate these signaling pathways [93]. Consistent with the specific activity of AVR3a on FLS2 internalization, DRP2 is specifically required for FLS2-endocytosis but not for BRI1. This supports a model in which different internalization pathways for receptor endocytosis may occur following flg22 and brassinosteroid perception. For instance, AVR3a may perturb DRP2 functions only at sites where the activated FLS2 receptor complex accumulates preventing downstream endocytosis. Our results suggest that BAK1/SERK3-associated membrane-bound receptors may be initially internalized via different endocytic pathways, which later on can converge at late endosomal compartments.

In animal systems, canonical dynamin proteins mediate pinching off of clathrin-coated vesicles from the membrane during constitutive endocytosis [52,55]. In Arabidopsis, the two canonical dynamins DRP2A and DRP2B have been shown to be genetically and functionally redundant and to play a role in endocytosis and gametophyte development [79,80,85]. However, Smith et al., [84] recently showed that DRP2B but not DRP2A, has distinct effects on flg22-signaling. DRP2B acts as a positive regulator of plant immunity to *Pseudomonas syringae* pv. *tomato* DC3000 while it functions as a negative regulator of RbohD/Ca^{2+}-dependent responses. In addition, FLS2 endocytosis is partially dependent on DRP2B but not DRP2A [84]. In this study, we also found that DRP2 is involved in FLS2 internalization and that it affects the accumulation of ROS upon PAMP treatment potentially placing this plant protein along the flg22-signaling pathway. However, these results do not indicate that FLS2 internalization is required for flg22 immune signaling responses. Indeed, suppression of ROS accumulation by DRP2 overexpression could be an indirect consequence of overexpressing an important component of plant cellular trafficking or may reflect pleiotropic effects on the PRRs or other components involved in ROS accumulation. Interestingly, the DRP2 family has expanded in *Solanaceae* compared to Arabidopsis, with no apparent orthologs of *DRP2A* and *DRP2B* (S7 Fig). Consistent with Smith et al., [84], our results also indicate that the DRP2 family has evolved multiple activities, with the *Solanaceous* DRP2 being involved in FLS2 but not BRI1 internalization (Fig 5 and panel C in S5 Fig). Possibly, plant DRPs have diversified to enable increased plasticity in response to biotic and abiotic stimuli. Further studies are clearly needed to fully understand the precise contributions of different plant DRPs to vesicle trafficking and flg22 responses.

In summary, we link the *P. infestans* effector AVR3a to a membrane complex that includes the vesicle trafficking protein DRP2. We found evidence supporting an active role of DRP2 during endocytosis of the classic pattern recognition receptor FLS2 following activation by the

flagellin-derived peptide flg22. Although the FLS2 co-receptor BAK1/SERK3 is required for basal immunity against the oomycete *P. infestans*, there is no evidence that FLS2, a receptor for bacterial flagellin, is activated and internalized during infection by this oomycete pathogen [39]. Therefore, AVR3a suppression of FLS2 responses and endocytosis may indicate that this effector targets a common node shared by FLS2 and a yet to be discovered PRR involved in oomycete immunity. Future studies are required to address this possibility and further determine the various mechanisms by which AVR3a perturbs PTI signaling.

Materials and Methods

Plant material

N. benthamiana and *A. thaliana* plants were grown and maintained under controlled environmental conditions at an average temperature of 23–25°C, with 45–65% humidity, and in long day conditions (16 hours of light) throughout the experiments. *N. benthamiana* and *A. thaliana* were transformed [94] with *A. tumefaciens* GV3101 or AGL1, respectively, carrying the following constructs: pBinplus::FLAG-AVR3a^{KI}, pBinplus::FLAG-AVR3a^{EM}, pBinplus::FLAG-AVR3a$^{KI\text{-}Y147del}$, or pBinplus::ΔGFP. Transformed plants were selected on Murashige-Skoog salts (MS) media containing selective antibiotic (kanamycin). Plates showing a segregation of 3:1 were selected and at least ten individual lines were selected to confirm expression of the transgene by western blot analysis with anti-FLAG antibody (SIGMA). Protein expression was confirmed for each individual plant once the plants reached the 3-week-old stage. Lines with different expression profiles were selected for further analysis. Transgenic lines used in this study were T4 and T3 for *N. benthamiana* and *A. thaliana* respectively.

The Sainsbury Laboratory and the John Innes Centre are registered with the Health and Safety Executive (site reference GM38) to use the laboratory premises, including growth rooms and controlled environment rooms (CERs) under containment level 1 and 2 for work involving genetically modified organisms. We confirm that our study did not involve any endangered or protected species.

A. tumefaciens-mediated transient gene expression assays in *N. benthamiana*

Agrobacterium tumefaciens (strain GV3101) carrying the desired T-DNA construct was grown overnight at 28°C in Luria-Bertani culture medium with the appropriate antibiotics. Cells were harvested by centrifugation at 8000 g and resuspended in agro-infiltration media [5 mM MES, 10 mM $MgCl_2$, pH 5.6] prior to syringe infiltration into leaves of 3–4 week-old *N. benthamiana* plants. Bacteria carrying each construct were infiltrated at a final OD_{600nm} of 0.3. Acetosyringone was added to the resuspended cultures at a final concentration of 150 μM and bacterial cultures were left at room temperature for 2 hours before infiltration.

Silencing experiments

A 445-nucleotide cDNA fragment of *NbDRP2–1* (*Nb05397*, position 2100–2545 bp) was cloned into pTV00 (between SpeI/KpnI sites) using the following primers *NbDRP2–1*_SpeI, 5'—GC GACTAGTATCAGCTCTAAAGGCGGTCA and *NbDRP2*–1_KpnI, 5'—AAAAGGTACCGC TGTTGGGCTACTTTCTGC to form TRV2-*NbDRP2*. TRV2 plasmids were transformed into *A. tumefaciens* GV3101. For VIGS assays, *A. tumefaciens* containing TRV2 and TRV1 plasmids were grown and prepared individually for agro-infiltration assays as previously described [95,96]. *A. tumefaciens* TRV1 and TRV2 were mixed in a 1:4 ratio to a final OD_{600} = 1.0 and infiltrated into 2-week-old *N. benthamiana* plants. Plants were analyzed and photographed

three weeks after inoculation. TRV-ΔGFP was used as a negative control and TRV-SU (reduced chlorophyll content of the silenced leaves) was used as a silencing control.

For transient silencing experiments, the same 445-nucleotide cDNA fragment of *NbDRP2–1* used for VIGS was cloned into pENTR/D-TOPO (Invitrogen) using the following primers: *NbDRP2–1*_hp_F2, 5'—CACCATCAGCTCTAAAGGCGGTCA and *NbDRP2–1*_hp_R2, 5'—GCTGTTGGGCTACTTTCTGC. The hairpin-silencing construct was generated by recombination into pHellesgate8 (Gateway LR recombination, Invitrogen) as described by Helliwell and Waterhouse [97]. The same procedure described above was used to generate the control silencing construct pHellsgate8-GUS (574 bp fragment size) using primers pH8_GUS_F1, 5'—CACCCCAGGCAGTTTTAACGATCAG and pH8_GUS_R1, 5'—GATTCACCACTTGC AAAGTCC. The final constructs were transformed into *A. tumefaciens* GV3101. Four-week-old *N. benthamiana* leaves were infiltrated with the hairpin silencing construct at a final OD_{600} = 0.3 either individually or co-expressed with a construct expressing the plant receptor under assessment. Further experiments (microscopy, analysis of gene silencing by qRT-PCR, PAMP elicitation and others described elsewhere in Materials and Methods) were performed three days after silencing.

Reactive oxygen species measurement

Generation of reactive oxygen species (ROS) was measured as previously described [91]. Briefly, leaf-discs (16–24 per treatment, 4 mm diameter) from pre-infiltrated or transgenic *N. benthamiana* leaves were floated 16 hours in 200 μl of water in a 96-well plate. Solution was replaced by a luminol/peroxidase mix [17 mg/ml (w/v) luminol (Sigma); 10 mg/ml horseradish peroxidase (Sigma)] supplied with either 100 nM flg22 peptide (EzBiolab), 100 nM elf18 peptide (EzBiolab), 5 μg/ml chitin (Sigma), or 10 μg/ml purified INF1[Pi] protein [36,98]. Luminescence was measured over time (up to 1320 min) using an ICCD photon-counting camera (Photek, East Sussex, UK) and analyzed using company software and Microsoft Excel.

Gene expression analysis

Transgenic *N. benthamiana* leaves expressing the constructs pBinplus::FLAG-AVR3a^{KI}, pBinplus::FLAG-AVR3a^{EM}, pBinplus::FLAG-AVR3a$^{KI\text{-}Y147del}$ or pBinplus::ΔGFP were treated for 0 and 180 minutes with flg22 (100 nM) or INF1[Pi] (10 μg/ml) on one side of the leaf and with Milli-Q water on the other side of the leaf as control. Total RNA was extracted using TRI reagent (Invitrogen) following manufacturer's instructions. DNase treatment (Ambion) was performed according to manufacturer's protocol and total RNA was quantified with a Nanodrop spectrophotometer (Thermo). 1.5 μg of DNase treated RNA was used for cDNA synthesis using SuperScript II reverse transcriptase (Invitrogen). qRT-PCR was performed with SYBR Green master mix (SIGMA) in triplicate per sample per gene. *NbEF1α* was used to normalize transcript abundance for the marker genes *NbACRE132*, *NbCYP71D20* and *NbACRE31* [72]. Primers used for amplification of *NbEF1α* and PAMP-induced marker genes in *N. benthamiana* have been reported previously [72].

qRT-PCR analysis of *N. benthamiana* genes *Nb05397* (*NbDRP2–1*), *Nb31648* (*NbDRP2–2*), *Nb11538* and *Nb09838* was performed with SYBR Green master mix (SIGMA) in triplicate per sample per gene, using primers silDyn_97–48_F, 5'—CGATCGAGGAATTGACACAA and silDyn_97–48_R, 5'—GCCTGAGCAGCAGATATTACG to detect *Nb05397* and *Nb31648* or 38s_F4, 5'—TAATCGAGCAGCTGCTGTG and 38s_3'UTR_R, 5'—TAGGATCAAGCA GCAACTG to detect *Nb11538* and *Nb09838*. *NbEF1α* [72] was used to normalize transcript abundance. 2.5 μg of DNase treated RNA was used for cDNA synthesis. Primers for *Nb11538* or *Nb09838* were predicted to specifically anneal at the 3'UTR of both sequences whereas

primers for *Nb05397* and *Nb31648* were predicted to specifically anneal along the GTPase domain of *Nb05397* and *Nb31648*.

Elicitor preparations

Chitin (crab shell chitin) and flg22 (QRLSTGSRINSAKDDAAGLQIA) peptides were purchased from SIGMA and EzBiolab, respectively and dissolved in ultrapure water. INF1[Pi] was purified from *P. infestans* 88069 by chromatography and the final working solution was dissolved in ultrapure water [36,98].

Co-immunoprecipitation assays and western blot analysis

N. benthamiana leaves expressing pTRBO::AVR3a^{KI}, pTRBO::AVR3a^{EM}, pTRBO::AVR3a$^{KI\text{-}Y147del}$, pTRBO::RFP or pTRBO::PcAVR3a-4 with pK7WGF2::NtDRP2–1 or pK7WG2–3xHA::NtDRP2–1 constructs were harvested at 3 days post infiltration and ground in liquid N_2 (see figure legends for more information). In Fig 2, pK7FWG2::FLS2 and pGWB14::BAK1 were co-infiltrated in *N. benthamiana* transgenic plants expressing pBinplus::FLAG-AVR3a^{KI} or pBinplus::ΔGFP and treated with flg22 (100 nM) or water for 15 minutes. Protein extraction and immunoprecipitation was performed with 50 μl of anti-FLAG resin (SIGMA) or 30 μl GFP-affinity matrix (Chromotek) as previously described [28,76]. Western blots analyses were performed as described by Oh et al., [99]. Protein blotting was done with monoclonal FLAG primary antibody (SIGMA) and anti-mouse as secondary antibody (SIGMA), or monoclonal GFP-HRP antibody (Santa Cruz) or monoclonal HA-HRP antibody (Santa Cruz).

Sample preparation and liquid chromatography-tandem mass spectrometry (LC-MS/MS) analysis was performed as described in Caillaud et al., [100]. Candidate AVR3a-associated proteins were identified from the peak lists searched on Mascot server v.2.4.1 (Matrix Science) against an in-house *N. benthamiana* database available upon request. We followed the same criteria in Caillaud et al., [100] for peptide identification. A complete list of all identified peptides for each AVR3a^{KI}-associated protein is provided in (S3 Table).

The pK7FWG2::FLS2 clone was generated from a pENTR::FLS2 and recombined into pK7FWG2 (GATEWAY, Invitrogen). The pGWB14::BAK1 clone is described in [28,71].

Cloning of *NtDRP2–1/2*

The AVR3a^{KI}-associated protein NCBE_074039.1 sequence identified through the LC-MS/MS analysis was used as query to search the TAIR9 database. *Arabidopsis thaliana* proteins DRP2A and DRP2B were then used as query to perform a TBLASTN in the *Nicotiana benthamiana* draft genome scaffolds and tomato genome database (Solanum Genomic Network (SGN)). Partial sequences were used to design the primers Dyn_F3, 5'—CACCATGGAAGCAATCGAGGAA TTGGAGCAG and Dyn_R2, 5'—TTATGATCTATAACCAGATCCAGACTGTGGTGG to amplify the open reading frame of the *Nicotiana tabacum* putative homologs of AtDRP2A/B from cDNA using Phusion proof reading polymerase (New England Biolabs). Amplicons were cloned into pENTR/D-TOPO (Invitrogen) and sequenced. Clones representing *NtDRP2–1* and *NtDRP2–2* were recombined into pK7WGF2, pK7WG2, and pK7WG2–3xHA to generate fusion proteins GFP-NtDRP2–1/2, non-tagged NtDRP2–1/2, and HA-NtDRP2–1/2, respectively. The final constructs were transformed into *A. tumefaciens* GV3101 and used for further analysis.

Phylogenetic analysis

In Arabidopsis, GTPases with a PH domain belong to the DRP2 subfamily [81]. Members of this subfamily, AtDRP2-A, AtDRP2-B, and the NtDRP2–1/2 cloned protein were used as

queries to search for homologs of DRP2 in Solanaceous and other dicot plants. We performed TBLASTN searches against the *Nicotiana benthamiana* genome version 0.4.4, the tomato genome International Tomato Annotation Group release 2.3, the potato genome Potato Genome Sequencing Consortium DM 3.4 (solanaceous genomes available at http://solgenomics.net) and the NCBI database. To reveal the evolutionary relationship of these proteins, an alignment of the conserved GTPase domain was constructed using the multiple alignment software MUSCLE [101] and a maximum likelihood (ML) tree was generated using the RAxML software [102]. To choose the best model for the ML tree, we estimated likelihoods of the trees constructed based on commonly used substitution models. The ML tree in S7 Fig was constructed with GAMMA model of rate heterogeneity and Whelan and Goldman model (WAG), since the tree based on WAG showed the highest likelihood. We performed 500 non-parametric bootstrap inferences. Bootstrap values over 70% are shown. All Arabidopsis DRPs were included in the analysis to ensure proper estimation of the closest homologs of AtDRP2A/B. Sequences identifiers are available in S3 Table.

Statistical analysis

Statistical analyses (One-way ANOVA, TukeyHSD test, Wilcoxon-Mann-Whitney Test, and Student's t Test) were performed using the software package R [103].

Confocal microscopy

Standard confocal microscopy was carried out in *N. benthamiana* epidermal cells 2 to 3 days post infiltration. Cut leaf pieces were mounted in water and analyzed with a Leica DM6000B/TCS SP5 microscope (Leica Microsystems, Germany) with laser excitation settings of 488-nm for eYFP and GFP and 561-nm for RFP. Fluorescent emissions were taken at 500–550 nm for GFP and 580–620 nm for RFP. The 63x water immersion objective was used to acquire all images. Image analysis was done with the Leica LAS AF software, ImageJ and Adobe Photoshop CS5. For all Z-stacks, a distance of 1 μm was set. For induction of FLS2 internalization, flg22 peptide (EzBiolab) was gently infiltrated into leaves expressing FLS2-GFP at a concentration of 100 μM [44] and imaging was done 80–150 minutes post elicitation. All images were processed with ImageJ (2.0) and endosomes were quantified based on naked-eye detection of distinct fluorescent signal in punctate structures per total image area (136 μm × 136 μm) using the multi-point tool. Propidium iodide (PI, SIGMA) staining was performed as previously described [104] with few modifications: leaf tissue was incubated in a solution of propidium iodide (200 μg/ml) for 10 minutes at room temperature, followed by three washing steps in ultra-pure water. To visualize PI-stained cells, laser excitation was set at 488-nm and fluorescence was detected between 598–650 nm.

Supporting Information

S1 Fig. All variants of AVR3a suppress flg22-mediated responses *in N. benthamiana* but show differential suppression of the marker gene *NbACRE31* after INF1 elicitation. (A, B) Total ROS production measured in relative light units (RLU) is expressed as percentage of the control treated with 100 nM flg22 over 45 minutes in transgenic plants of *N. benthamiana* (A) or *A. thaliana* (B). Plants were stably transformed with the following constructs: FLAG-AVR3a^{KI} (red), FLAG-AVR3a^{EM} (blue), FLAG-AVR3a$^{KI\text{-}Y147del}$ (grey) or vector control (ΔGFP) (green). Values are average ± SE (n = 24). Statistical significance was evaluated in comparison to the control by one-way ANOVA followed by TukeyHSD test. (C, D) Expression of the marker gene *NbACRE31* was assessed by qRT-PCR at time 0 and 180 minutes after elicitation with 100 nM flg22 (C) or 10 μg/ml INF1[Pi] (D) and normalized by NbEF1α gene expression.

Results are average ± SE (n = 3 technical replicates). AVR3a variants were transiently expressed in *N. benthamiana* using the following constructs: FLAG-AVR3a^{KI} (red), FLAG-AVR3a^{EM} (blue), FLAG-AVR3a$^{KI\text{-}Y147del}$ (grey) or vector control (ΔGFP) (green). (E, F) Western blots probed with anti-FLAG antibody after flg22 (E) or INF1 (F) treatment detected total protein expression of AVR3a variants.
(TIF)

S2 Fig. AVR3a suppresses elf18-ROS production but does not affect chitin-triggered ROS accumulation. (A, B) *N. benthamiana* agro-infiltrated with FLAG-AVR3a^{KI} (red), FLAG-AVR3a^{EM} (blue), FLAG-AVR3a$^{KI\text{-}Y147del}$ (grey) or vector control (ΔGFP) (green). Leaf discs were incubated in an elf18 (A) or chitin (B) containing solution and ROS production was measured in relative light units (RLU) over time. Letters above the graph indicate statistical significant differences at $P < 0.05$ assessed by one-way ANOVA followed by TukeyHSD test. No statistical significance was found for group b ($P = 0.068$). Similar results were observed in two independent experiments.
(TIF)

S3 Fig. AVR3a does not alter the subcellular localization of the surface receptors EFR or CERK1. Transient co-expression at 2.5 days post infiltration in *N. benthamiana* of EFR-YFP-HA or CERK1-GFP with FLAG-AVR3a^{KI} or FLAG-AVR3a^{EM} or FLAG-AVR3a$^{KI\text{-}Y147del}$ or vector control (ΔGFP) as indicated. Confocal microscopy shows that the plasma membrane localization of EFR-YFP or CERK1-GFP was not altered by the presence of variants of AVR3a. Bar = 25 μm.
(TIF)

S4 Fig. AVR3a partially suppresses the endosomal localization of the activated FLS2 receptor. Enlarged confocal images showed in Fig 3. White arrowheads and inset image indicate FLS2 endosomes. Bar = 25 μm.
(TIF)

S5 Fig. BRI1 constitutive internalization is not modified by AVR3a or by silencing *NbDRP2–1/2*. (A) Confocal microscopy at 2.5 days post infiltration (dpi) in *N. benthamiana* epidermal leaf cells transiently or stably expressing FLAG-AVR3a^{KI} and infiltrated with BRI1-GFP. AVR3a did not alter the plasma membrane subcellular localization of BRI1 or its constitutive endosomal localization (green dots). Bar = 50 μm. Plastids auto-fluorescence (purple) is shown. (B) Quantification of the effect of AVR3a on AtBRI1 endocytosis. Scatter plots show the number of BRI1-GFP endosomes per total image area from 3 independent biological experiments. Vector control (ΔGFP) n = 10, FLAG-AVR3a^{KI} n = 14. No statistical difference was found as assessed by Wilcoxon-Mann-Whitney Test. $P = 0.3$. (C) BRI1-GFP was co-expressed with a hairpin-silencing construct for *NbDRP2–1/2* or the vector RNAi-GUS and confocal imaging was done at 2.5 dpi. Reduced levels of expression of *NbDRP2–1/2* did not change BRI1-GFP intracellular vesicle-like (green dots) or plasma membrane localization. Bar = 50 μm. Plastids auto-fluorescence (purple) is shown. All images are a maximum projection of 21 slices taken at 1-μm intervals. Same confocal settings were used to acquire all images. (D) Validation of *NbDRP2–1/2* silencing by RT-PCR in leaf-discs collected from the same leaves used for microscopy. (E) Quantification of the effect of RNAi-*NbDRP2–1/2* on AtBRI1 endocytosis. Scatter plots show the number of BRI1-GFP endosomes per total image area from 3 independent biological experiments. RNAi-GUS n = 27, RNAi-*NbDRP2–1/2* n = 27. No statistical difference was found as assessed by Student's t test. $P = 0.1$.
(TIF)

S6 Fig. *A. thaliana* dynamin GTPase DRP2A/B homologs in *N. tabacum*. ClustalW alignment shows Arabidopsis DRP2A and DRP2B dynamin GTPase proteins and homologs in *N. tabacum*. Amino acid residues are shaded dark grey if identical and a lighter shade of grey if similar. Sequences were viewed in Jalview. Full-length sequences were used for the alignment. Canonical domains previously described for large dynamin GTPase are shown.
(TIF)

S7 Fig. Cladogram of dynamin related proteins (DRP). Phylogenetic tree of dynamin-related proteins (DRP) from *A. thaliana* (red), *N. benthamiana* (green), tomato (purple), potato (yellow), *N. tabacum* (dark blue), *P. trichocarpa* (pink), *V. vinifera* (black) and *M. truncatula* (light blue). The conserved GTPase-domain of DRP proteins was aligned by MUSCLE and analyzed with RAxML to construct a phylogenetic tree using the maximum likelihood method. Branch length represents the estimated genetic distance. Bootstrap values for 500 replicates are shown. The sequence identifiers are from the Solgenomics, NCBI and Arabidopsis database. Green asterisks indicate the homologs of Arabidopsis DRP2A and DRP2B in *N. benthamiana* targeted by silencing in this study.
(TIF)

S8 Fig. *N. tabacum* dynamin (DRP2–1) is a modular protein localized to the plasma membrane and cytosol in *N. benthamiana*. (A) Schematic representation of *N. tabacum* dynamin proteins (NtDRP2–1 and NtDRP2–2) and their domain organization: GTPase domain (G domain), Pleckstrin homology domain (PH), GTPase effector domain (GED), and a proline-rich domain (PRD). (B, C) Confocal microscopy in *N. benthamiana* pavement cells of *Agrobacterium*-mediated expressing NtDRP2–1/2 GFP fusions. GFP-NtDRP2–1 or GFP-NtDRP2–2 primarily localized to the plasma membrane as confirmed by plasmolysis (C), far right end. (C) GFP-NtDRP2–1 and GFP-NtDRP2–2 also localized in punctuate, small vesicle-like structures. Scale bar values are shown in each picture. Representative confocal images were taken at 2.5 days post infiltration. Plastids auto-fluorescence (purple) is shown.
(TIF)

S9 Fig. *P. capsici* effector AVR3a-4 does not associate with NtDRP2–1 *in planta*. (A) *Phytophthora capsici* AVR3a-4 effector weakly co-immunoprecipitates with NtDRP2–1 *in planta*. HA-NtDRP2–1 was transiently co-expressed with FLAG-AVR3a^{KI}, FLAG-PcAVR3a-4 or FLAG-RFP (control) in *N. benthamiana* and immunoprecipitated with anti-FLAG antiserum (SIGMA). Immunoprecipitates and total protein extracts were immunoblotted with the appropriate antisera. (B) Oxidative burst triggered by 100 nM flg22 in *N. benthamiana* agroinfiltrated with members of the *Avr3a* family FLAG-AVR3a^{KI}, FLAG-PcAVR3a-4 or FLAG-RFP (control). ROS production was measured in relative light units (RLU) over time and depicted relative to the total ROS burst of the control. Values are average ± SE (n = 16). Statistical significance was evaluated in comparison to the control by one-way ANOVA followed by TukeyHSD test. *** $P < 0.001$. Experiment was repeated 3 times with similar results.
(TIF)

S10 Fig. Impact of systemically silencing *NbDRP2–1/2* in *N. benthamiana* using VIGS. *N. benthamiana* plants were silenced using tobacco rattle virus vectors harboring a partial sequence of *NbDRP2–1* (TRV::*NbDRP2–1/2* Fragment I or TRV::*NbDRP2–1/2* Fragment II) or an empty cloning site (TRV::*GFP*). Pictures were taken 2.5 weeks after the initial infiltration with the silencing constructs.
(TIF)

S11 Fig. RNAi-mediated transient silencing of *NbDRP2–1/2* in *N. benthamiana* does not compromise cell viability. (A) Schematic representation of *NbDRP2–1/2* (*Nb05397* and *Nb31648*) showing the canonical dynamin domains and the sequence region targeted by the silencing fragment. (B) Constructs carrying a hairpin plasmid (pHellsgate 8) targeting *NbDRP2–1/2* or GUS (RNAi-*NbDRP2–1/2* and RNAi-GUS, respectively) were infiltrated in *N. benthamiana* and the expression of *N. benthamiana* homologs of *AtDRP2A/B* was assessed by qRT-PCR at three days post silencing. The silencing fragment targeting part of the pleckstrin homology domain (PH, green) and the GTPase effector domain (blue) specifically knocks down the expression of *Nb05397* and *Nb31648* (*NbDRP2–1* and *NbDRP2–2*) but not the expression of *Nb11538* or *Nb09838*. Gene expression was normalized to *NbEF1α*. (C) The *NbDRP2–1/2* genes were transiently silenced in *N. benthamiana* and at three days post silencing, the epidermal cells were stained for 5 minutes with a solution of propidium iodide (PI). Auto-fluorescence of chloroplasts (purple) is shown. The absence of PI fluorescence in the cell nucleus (dashed white lines) indicates that the cells are still viable. Bar = 25 μm.
(TIF)

S12 Fig. ROS accumulation after flg22 treatment in *NbDRP2*-silenced *N. benthamiana* leaves.
(TIF)

S1 Table. Plant proteins that associate with AVR3a^{KI} *in planta*.
(XLSX)

S2 Table. Sequence identifiers used in S6 Fig.
(XLSX)

S3 Table. AVR3a^{KI}-associated proteins identified peptides by LC-MS/MS.
(XLSX)

Acknowledgments

We thank Silke Robatzek, Martina Beck and Malick Mbengue for advice on confocal microscopy and FLS2 internalization assays and for critical comments on our silencing experiments. We are grateful to Matthew Smoker for generating the AVR3a transgenic plants, Volker Lipka and Markus Albert for providing the constructs CERK1-GFP and BRI1-GFP, respectively, and Benjamin Schwessinger and Cyril Zipfel for providing the pENTR-FLS2 clone and for fruitful discussions. We also thank Jacqueline Monaghan, Joe Win, Khaoula Belhaj and Yasin Dagdas for critical reading of the manuscript.

Author Contributions

Conceived and designed the experiments: ACG S. Schwizer TOB SK. Performed the experiments: ACG S. Schwizer JS JIBB S. Schornack AMEJ TOB. Analyzed the data: ACG JS KY BP S. Schornack AMEJ TOB SK. Contributed reagents/materials/analysis tools: ACG S. Schwizer JS BP JIBB AMEJ TOB SK. Wrote the paper: ACG TOB SK.

References

1. Vorholt JA (2012) Microbial life in the phyllosphere. Nat Rev Microbiol 10: 828–840. doi: 10.1038/nrmicro2910 PMID: 23154261
2. Bulgarelli D, Schlaeppi K, Spaepen S, Ver Loren van Themaat E, Schulze-Lefert P (2013) Structure and functions of the bacterial microbiota of plants. Annu Rev Plant Biol 64: 807–838. doi: 10.1146/annurev-arplant-050312-120106 PMID: 23373698

3. Dodds PN, Rathjen JP (2010) Plant immunity: towards an integrated view of plant-pathogen interactions. Nat Rev Genet 11: 539–548. doi: 10.1038/nrg2812 PMID: 20585331
4. Win J, Chaparro-Garcia A, Belhaj K, Saunders DG, Yoshida K, Dong S, et al. (2012) Effector biology of plant-associated organisms: concepts and perspectives. Cold Spring Harb Symp Quant Biol 77: 235–247. doi: 10.1101/sqb.2012.77.015933 PMID: 23223409
5. Monaghan J, Zipfel C (2012) Plant pattern recognition receptor complexes at the plasma membrane. Curr Opin Plant Biol 15: 349–357. doi: 10.1016/j.pbi.2012.05.006 PMID: 22705024
6. Boller T, Felix G (2009) A renaissance of elicitors: perception of microbe-associated molecular patterns and danger signals by pattern-recognition receptors. Annu Rev Plant Biol 60: 379–406. doi: 10.1146/annurev.arplant.57.032905.105346 PMID: 19400727
7. Nicaise V, Roux M, Zipfel C (2009) Recent advances in PAMP-triggered immunity against bacteria: pattern recognition receptors watch over and raise the alarm. Plant Physiol 150: 1638–1647. doi: 10.1104/pp.109.139709 PMID: 19561123
8. Segonzac C, Zipfel C (2011) Activation of plant pattern-recognition receptors by bacteria. Curr Opin Microbiol 14: 54–61. doi: 10.1016/j.mib.2010.12.005 PMID: 21215683
9. Macho AP, Zipfel C (2014) Plant PRRs and the activation of innate immune signaling. Mol Cell 54: 263–272. doi: 10.1016/j.molcel.2014.03.028 PMID: 24766890
10. Hogenhout SA, Van der Hoorn RA, Terauchi R, Kamoun S (2009) Emerging concepts in effector biology of plant-associated organisms. Mol Plant Microbe Interact 22: 115–122. doi: 10.1094/MPMI-22-2-0115 PMID: 19132864
11. Boller T, He SY (2009) Innate immunity in plants: an arms race between pattern recognition receptors in plants and effectors in microbial pathogens. Science 324: 742–744. doi: 10.1126/science.1171647 PMID: 19423812
12. Lu D, He P, Shan L (2010) Bacterial effectors target BAK1-associated receptor complexes: One stone two birds. Commun Integr Biol 3: 80–83. PMID: 20585495
13. Macho AP, Zipfel C (2014) Targeting of plant pattern recognition receptor-triggered immunity by bacterial type-III secretion system effectors. Curr Opin Microbiol 23C: 14–22.
14. Bozkurt TO, Schornack S, Banfield MJ, Kamoun S (2012) Oomycetes, effectors, and all that jazz. Curr Opin Plant Biol 15: 483–492. doi: 10.1016/j.pbi.2012.03.008 PMID: 22483402
15. Rafiqi M, Ellis JG, Ludowici VA, Hardham AR, Dodds PN (2012) Challenges and progress towards understanding the role of effectors in plant-fungal interactions. Curr Opin Plant Biol 15: 477–482. doi: 10.1016/j.pbi.2012.05.003 PMID: 22658704
16. Rovenich H, Boshoven JC, Thomma BP (2014) Filamentous pathogen effector functions: of pathogens, hosts and microbiomes. Curr Opin Plant Biol 20: 96–103. doi: 10.1016/j.pbi.2014.05.001 PMID: 24879450
17. Okmen B, Doehlemann G (2014) Inside plant: biotrophic strategies to modulate host immunity and metabolism. Curr Opin Plant Biol 20: 19–25. doi: 10.1016/j.pbi.2014.03.011 PMID: 24780462
18. Zipfel C (2014) Plant pattern-recognition receptors. Trends Immunol 35: 345–351. doi: 10.1016/j.it.2014.05.004 PMID: 24946686
19. Gomez-Gomez L, Boller T (2000) FLS2: an LRR receptor-like kinase involved in the perception of the bacterial elicitor flagellin in Arabidopsis. Mol Cell 5: 1003–1011. PMID: 10911994
20. Chinchilla D, Bauer Z, Regenass M, Boller T, Felix G (2006) The Arabidopsis receptor kinase FLS2 binds flg22 and determines the specificity of flagellin perception. Plant Cell 18: 465–476. PMID: 16377758
21. Zipfel C, Kunze G, Chinchilla D, Caniard A, Jones JD, Boller T, et al. (2006) Perception of the bacterial PAMP EF-Tu by the receptor EFR restricts *Agrobacterium*-mediated transformation. Cell 125: 749–760. PMID: 16713565
22. Miya A, Albert P, Shinya T, Desaki Y, Ichimura K, Shirasu K, et al. (2007) CERK1, a LysM receptor kinase, is essential for chitin elicitor signaling in Arabidopsis. Proc Natl Acad Sci U S A 104: 19613–19618. PMID: 18042724
23. Petutschnig EK, Jones AM, Serazetdinova L, Lipka U, Lipka V (2010) The lysin motif receptor-like kinase (LysM-RLK) CERK1 is a major chitin-binding protein in *Arabidopsis thaliana* and subject to chitin-induced phosphorylation. J Biol Chem 285: 28902–28911. doi: 10.1074/jbc.M110.116657 PMID: 20610395
24. Cao Y, Liang Y, Tanaka K, Nguyen CT, Jedrzejczak RP, Joachimiak A, et al. (2014) The kinase LYK5 is a major chitin receptor in Arabidopsis and forms a chitin-induced complex with related kinase CERK1. Elife 3.

25. Chinchilla D, Zipfel C, Robatzek S, Kemmerling B, Nurnberger T, Jones JD, et al. (2007) A flagellin-induced complex of the receptor FLS2 and BAK1 initiates plant defence. Nature 448: 497–500. PMID: 17625569

26. Heese A, Hann DR, Gimenez-Ibanez S, Jones AM, He K, Li J, et al. (2007) The receptor-like kinase SERK3/BAK1 is a central regulator of innate immunity in plants. Proc Natl Acad Sci U S A 104: 12217–12222. PMID: 17626179

27. Schulze B, Mentzel T, Jehle AK, Mueller K, Beeler S, Boller T, et al. (2010) Rapid heteromerization and phosphorylation of ligand-activated plant transmembrane receptors and their associated kinase BAK1. J Biol Chem 285: 9444–9451. doi: 10.1074/jbc.M109.096842 PMID: 20103591

28. Roux M, Schwessinger B, Albrecht C, Chinchilla D, Jones A, Holton N, et al. (2011) The Arabidopsis leucine-rich repeat receptor-like kinases BAK1/SERK3 and BKK1/SERK4 are required for innate immunity to hemibiotrophic and biotrophic pathogens. Plant Cell 23: 2440–2455. doi: 10.1105/tpc.111.084301 PMID: 21693696

29. Sun Y, Li L, Macho AP, Han Z, Hu Z, Zipfel C, et al. (2013) Structural basis for flg22-induced activation of the Arabidopsis FLS2-BAK1 immune complex. Science 342: 624–628. doi: 10.1126/science.1243825 PMID: 24114786

30. Nam KH, Li J (2002) BRI1/BAK1, a receptor kinase pair mediating brassinosteroid signaling. Cell 110: 203–212. PMID: 12150928

31. Li J, Wen J, Lease KA, Doke JT, Tax FE, Walker JC (2002) BAK1, an Arabidopsis LRR receptor-like protein kinase, interacts with BRI1 and modulates brassinosteroid signaling. Cell 110: 213–222. PMID: 12150929

32. Russinova E, Borst JW, Kwaaitaal M, Cano-Delgado A, Yin Y, Chory J, et al. (2004) Heterodimerization and endocytosis of Arabidopsis brassinosteroid receptors BRI1 and AtSERK3 (BAK1). Plant Cell 16: 3216–3229. PMID: 15548744

33. Chinchilla D, Shan L, He P, de Vries S, Kemmerling B (2009) One for all: the receptor-associated kinase BAK1. Trends Plant Sci 14: 535–541. doi: 10.1016/j.tplants.2009.08.002 PMID: 19748302

34. Fradin EF, Zhang Z, Juarez Ayala JC, Castroverde CD, Nazar RN, Robb J, et al. (2009) Genetic dissection of *Verticillium* wilt resistance mediated by tomato Ve1. Plant Physiol 150: 320–332. doi: 10.1104/pp.109.136762 PMID: 19321708

35. Bar M, Sharfman M, Ron M, Avni A (2010) BAK1 is required for the attenuation of ethylene-inducing xylanase (Eix)-induced defense responses by the decoy receptor LeEix1. Plant J 63: 791–800. doi: 10.1111/j.1365-313X.2010.04282.x PMID: 20561260

36. Chaparro-Garcia A, Wilkinson RC, Gimenez-Ibanez S, Findlay K, Coffey MD, Zipfel C, et al. (2011) The receptor-like kinase SERK3/BAK1 is required for basal resistance against the late blight pathogen *Phytophthora infestans* in *Nicotiana benthamiana*. PLoS One 6: e16608. doi: 10.1371/journal.pone.0016608 PMID: 21304602

37. Larroque M, Belmas E, Martinez T, Vergnes S, Ladouce N, Lafitte C, et al. (2013) Pathogen-associated molecular pattern-triggered immunity and resistance to the root pathogen *Phytophthora parasitica* in Arabidopsis. J Exp Bot 64: 3615–3625. doi: 10.1093/jxb/ert195 PMID: 23851194

38. Lu YJ, Schornack S, Spallek T, Geldner N, Chory J, Schellmann S, et al. (2012) Patterns of plant subcellular responses to successful oomycete infections reveal differences in host cell reprogramming and endocytic trafficking. Cell Microbiol 14: 682–697. doi: 10.1111/j.1462-5822.2012.01751.x PMID: 22233428

39. Bozkurt TO, Belhaj K, Dagdas YF, Chaparro-Garcia A, Wu CH, Cano LM, et al. (2014) Rerouting of plant late endocytic trafficking towards a pathogen interface. Traffic.

40. Robatzek S (2014) Endocytosis: At the Crossroads of Pattern Recognition Immune Receptors and Pathogen Effectors: Springer Berlin Heidelberg.

41. Beck M, Zhou J, Faulkner C, MacLean D, Robatzek S (2012) Spatio-temporal cellular dynamics of the Arabidopsis flagellin receptor reveal activation status-dependent endosomal sorting. Plant Cell 24: 4205–4219. doi: 10.1105/tpc.112.100263 PMID: 23085733

42. Robatzek S, Chinchilla D, Boller T (2006) Ligand-induced endocytosis of the pattern recognition receptor FLS2 in Arabidopsis. Genes Dev 20: 537–542. PMID: 16510871

43. Salomon S, Robatzek S (2006) Induced Endocytosis of the Receptor Kinase FLS2. Plant Signal Behav 1: 293–295. PMID: 19704570

44. Choi SW, Tamaki T, Ebine K, Uemura T, Ueda T, Nakano A (2013) RABA members act in distinct steps of subcellular trafficking of the FLAGELLIN SENSING2 receptor. Plant Cell 25: 1174–1187. doi: 10.1105/tpc.112.108803 PMID: 23532067

45. Platta HW, Stenmark H (2011) Endocytosis and signaling. Curr Opin Cell Biol 23: 393–403. doi: 10.1016/j.ceb.2011.03.008 PMID: 21474295

46. Teis D, Taub N, Kurzbauer R, Hilber D, de Araujo ME, Erlacher M, et al. (2006) p14-MP1-MEK1 signaling regulates endosomal traffic and cellular proliferation during tissue homeostasis. J Cell Biol 175: 861–868. PMID: 17178906

47. Hisata S, Sakisaka T, Baba T, Yamada T, Aoki K, Matsuda M, et al. (2007) Rap1-PDZ-GEF1 interacts with a neurotrophin receptor at late endosomes, leading to sustained activation of Rap1 and ERK and neurite outgrowth. J Cell Biol 178: 843–860. PMID: 17724123

48. Chockalingam A, Brooks JC, Cameron JL, Blum LK, Leifer CA (2009) TLR9 traffics through the Golgi complex to localize to endolysosomes and respond to CpG DNA. Immunol Cell Biol 87: 209–217. doi: 10.1038/icb.2008.101 PMID: 19079358

49. Ewald SE, Lee BL, Lau L, Wickliffe KE, Shi GP, Chapman HA, et al. (2008) The ectodomain of Toll-like receptor 9 is cleaved to generate a functional receptor. Nature 456: 658–662. doi: 10.1038/nature07405 PMID: 18820679

50. Irani NG, Di Rubbo S, Mylle E, Van den Begin J, Schneider-Pizon J, Hnilikova J, et al. (2012) Fluorescent castasterone reveals BRI1 signaling from the plasma membrane. Nat Chem Biol 8: 583–589. doi: 10.1038/nchembio.958 PMID: 22561410

51. Geldner N, Hyman DL, Wang X, Schumacher K, Chory J (2007) Endosomal signaling of plant steroid receptor kinase BRI1. Genes Dev 21: 1598–1602. PMID: 17578906

52. Doherty GJ, McMahon HT (2009) Mechanisms of endocytosis. Annu Rev Biochem 78: 857–902. doi: 10.1146/annurev.biochem.78.081307.110540 PMID: 19317650

53. Sigismund S, Confalonieri S, Ciliberto A, Polo S, Scita G, Di Fiore PP (2012) Endocytosis and signaling: cell logistics shape the eukaryotic cell plan. Physiol Rev 92: 273–366. doi: 10.1152/physrev.00005.2011 PMID: 22298658

54. Di Rubbo S, Irani NG, Kim SY, Xu ZY, Gadeyne A, Dejonghe W, et al. (2013) The clathrin adaptor complex AP-2 mediates endocytosis of brassinosteroid insensitive1 in Arabidopsis. Plant Cell 25: 2986–2997. doi: 10.1105/tpc.113.114058 PMID: 23975899

55. Ferguson SM, De Camilli P (2012) Dynamin, a membrane-remodelling GTPase. Nat Rev Mol Cell Biol 13: 75–88. doi: 10.1038/nrm3266 PMID: 22233676

56. Basquin C, Malarde V, Mellor P, Anderson DH, Meas-Yedid V, Olivo-Marin JC, et al. (2013) The signalling factor PI3K is a specific regulator of the clathrin-independent dynamin-dependent endocytosis of IL-2 receptors. J Cell Sci 126: 1099–1108. doi: 10.1242/jcs.110932 PMID: 23345407

57. Robinson DG, Jiang L, Schumacher K (2008) The endosomal system of plants: charting new and familiar territories. Plant Physiol 147: 1482–1492. doi: 10.1104/pp.108.120105 PMID: 18678740

58. Chen X, Irani NG, Friml J (2011) Clathrin-mediated endocytosis: the gateway into plant cells. Curr Opin Plant Biol 14: 674–682. doi: 10.1016/j.pbi.2011.08.006 PMID: 21945181

59. Fisher MC, Henk DA, Briggs CJ, Brownstein JS, Madoff LC, McCraw SL, et al. (2012) Emerging fungal threats to animal, plant and ecosystem health. Nature 484: 186–194. doi: 10.1038/nature10947 PMID: 22498624

60. Petre B, Kamoun S (2014) How do filamentous pathogens deliver effector proteins into plant cells? PLoS Biol 12: e1001801. doi: 10.1371/journal.pbio.1001801 PMID: 24586116

61. Boutemy LS, King SR, Win J, Hughes RK, Clarke TA, Blumenschein TM, et al. (2011) Structures of *Phytophthora* RXLR effector proteins: a conserved but adaptable fold underpins functional diversity. J Biol Chem 286: 35834–35842. doi: 10.1074/jbc.M111.262303 PMID: 21813644

62. Win J, Krasileva KV, Kamoun S, Shirasu K, Staskawicz BJ, Banfield MJ (2012) Sequence divergent RXLR effectors share a structural fold conserved across plant pathogenic oomycete species. PLoS Pathog 8: e1002400. doi: 10.1371/journal.ppat.1002400 PMID: 22253591

63. Armstrong MR, Whisson SC, Pritchard L, Bos JI, Venter E, Avrova AO, et al. (2005) An ancestral oomycete locus contains late blight avirulence gene AVR3a, encoding a protein that is recognized in the host cytoplasm. Proc Natl Acad Sci U S A 102: 7766–7771. PMID: 15894622

64. Bos JI, Kanneganti TD, Young C, Cakir C, Huitema E, Win J, et al. (2006) The C-terminal half of *Phytophthora infestans* RXLR effector AVR3a is sufficient to trigger R3a-mediated hypersensitivity and suppress INF1-induced cell death in *Nicotiana benthamiana*. Plant J 48: 165–176. PMID: 16965554

65. Bos JI, Chaparro-Garcia A, Quesada-Ocampo LM, McSpadden Gardener BB, Kamoun S (2009) Distinct amino acids of the *Phytophthora infestans* effector AVR3a condition activation of R3a hypersensitivity and suppression of cell death. Mol Plant Microbe Interact 22: 269–281. doi: 10.1094/MPMI-22-3-0269 PMID: 19245321

66. Haas BJ, Kamoun S, Zody MC, Jiang RH, Handsaker RE, Cano LM, et al. (2009) Genome sequence and analysis of the Irish potato famine pathogen *Phytophthora infestans*. Nature 461: 393–398. doi: 10.1038/nature08358 PMID: 19741609

67. Bos JI, Armstrong MR, Gilroy EM, Boevink PC, Hein I, Taylor RM, et al. (2010) *Phytophthora infestans* effector AVR3a is essential for virulence and manipulates plant immunity by stabilizing host E3 ligase CMPG1. Proc Natl Acad Sci U S A 107: 9909–9914. doi: 10.1073/pnas.0914408107 PMID: 20457921

68. Engelhardt S, Boevink PC, Armstrong MR, Ramos MB, Hein I, Birch PR (2012) Relocalization of late blight resistance protein R3a to endosomal compartments is associated with effector recognition and required for the immune response. Plant Cell 24: 5142–5158. doi: 10.1105/tpc.112.104992 PMID: 23243124

69. Gilroy EM, Taylor RM, Hein I, Boevink P, Sadanandom A, Birch PR (2011) CMPG1-dependent cell death follows perception of diverse pathogen elicitors at the host plasma membrane and is suppressed by *Phytophthora infestans* RXLR effector AVR3a. New Phytol 190: 653–666. doi: 10.1111/j.1469-8137.2011.03643.x PMID: 21348873

70. Navarro L, Zipfel C, Rowland O, Keller I, Robatzek S, Boller T, et al. (2004) The transcriptional innate immune response to flg22. Interplay and overlap with Avr gene-dependent defense responses and bacterial pathogenesis. Plant Physiol 135: 1113–1128. PMID: 15181213

71. Schwessinger B, Roux M, Kadota Y, Ntoukakis V, Sklenar J, Jones A, et al. (2011) Phosphorylation-dependent differential regulation of plant growth, cell death, and innate immunity by the regulatory receptor-like kinase BAK1. PLoS Genet 7: e1002046. doi: 10.1371/journal.pgen.1002046 PMID: 21593986

72. Segonzac C, Feike D, Gimenez-Ibanez S, Hann DR, Zipfel C, Rathjen JP (2011) Hierarchy and roles of pathogen-associated molecular pattern-induced responses in *Nicotiana benthamiana*. Plant Physiol 156: 687–699. doi: 10.1104/pp.110.171249 PMID: 21478366

73. Gohre V, Spallek T, Haweker H, Mersmann S, Mentzel T, Boller T, et al. (2008) Plant pattern-recognition receptor FLS2 is directed for degradation by the bacterial ubiquitin ligase AvrPtoB. Curr Biol 18: 1824–1832. doi: 10.1016/j.cub.2008.10.063 PMID: 19062288

74. Shan L, He P, Li J, Heese A, Peck SC, Nurnberger T, et al. (2008) Bacterial effectors target the common signaling partner BAK1 to disrupt multiple MAMP receptor-signaling complexes and impede plant immunity. Cell Host Microbe 4: 17–27. doi: 10.1016/j.chom.2008.05.017 PMID: 18621007

75. Xiang T, Zong N, Zou Y, Wu Y, Zhang J, Xing W, et al. (2008) *Pseudomonas syringae* effector AvrPto blocks innate immunity by targeting receptor kinases. Curr Biol 18: 74–80. PMID: 18158241

76. Win J, Kamoun S, Jones AM (2011) Purification of effector-target protein complexes via transient expression in *Nicotiana benthamiana*. Methods Mol Biol 712: 181–194. doi: 10.1007/978-1-61737-998-7_15 PMID: 21359809

77. Praefcke GJ, McMahon HT (2004) The dynamin superfamily: universal membrane tubulation and fission molecules? Nat Rev Mol Cell Biol 5: 133–147. PMID: 15040446

78. Jin JB, Kim YA, Kim SJ, Lee SH, Kim DH, Cheong GW, et al. (2001) A new dynamin-like protein, ADL6, is involved in trafficking from the trans-Golgi network to the central vacuole in Arabidopsis. Plant Cell 13: 1511–1526. PMID: 11449048

79. Taylor NG (2011) A role for Arabidopsis dynamin related proteins DRP2A/B in endocytosis; DRP2 function is essential for plant growth. Plant Mol Biol 76: 117–129. doi: 10.1007/s11103-011-9773-1 PMID: 21461976

80. Backues SK, Korasick DA, Heese A, Bednarek SY (2010) The Arabidopsis dynamin-related protein2 family is essential for gametophyte development. Plant Cell 22: 3218–3231. doi: 10.1105/tpc.110.077727 PMID: 20959563

81. Hong Z, Bednarek SY, Blumwald E, Hwang I, Jurgens G, Menzel D, et al. (2003) A unified nomenclature for Arabidopsis dynamin-related large GTPases based on homology and possible functions. Plant Mol Biol 53: 261–265. PMID: 14750516

82. Fujimoto M, Arimura S, Nakazono M, Tsutsumi N (2008) Arabidopsis dynamin-related protein DRP2B is co-localized with DRP1A on the leading edge of the forming cell plate. Plant Cell Rep 27: 1581–1586. doi: 10.1007/s00299-008-0583-0 PMID: 18612642

83. Fujimoto M, Arimura S, Ueda T, Takanashi H, Hayashi Y, Nakano A, et al. (2010) Arabidopsis dynamin-related proteins DRP2B and DRP1A participate together in clathrin-coated vesicle formation during endocytosis. Proc Natl Acad Sci U S A 107: 6094–6099. doi: 10.1073/pnas.0913562107 PMID: 20231465

84. Smith JM, Leslie ME, Robinson SJ, Korasick DA, Zhang T, Backues SK, et al. (2014) Loss of *Arabidopsis thaliana* Dynamin-Related Protein 2B Reveals Separation of Innate Immune Signaling Pathways. PLoS Pathog 10: e1004578. doi: 10.1371/journal.ppat.1004578 PMID: 25521759

85. Huang J, Fujimoto M, Fujiwara M, Fukao Y, Arimura S, Tsutsumi N (2015) Arabidopsis dynamin-related proteins, DRP2A and DRP2B, function coordinately in post-Golgi trafficking. Biochem Biophys Res Commun 456: 238–244. doi: 10.1016/j.bbrc.2014.11.065 PMID: 25462567

86. Yaeno T, Li H, Chaparro-Garcia A, Schornack S, Koshiba S, Watanabe S, et al. (2011) Phosphatidylinositol monophosphate-binding interface in the oomycete RXLR effector AVR3a is required for its stability in host cells to modulate plant immunity. Proc Natl Acad Sci U S A 108: 14682–14687. doi: 10.1073/pnas.1106002108 PMID: 21821794

87. Schafer DA (2004) Regulating actin dynamics at membranes: a focus on dynamin. Traffic 5: 463–469. PMID: 15180823

88. Zheng X, McLellan H, Fraiture M, Liu X, Boevink PC, Gilroy EM, et al. (2014) Functionally redundant RXLR effectors from *Phytophthora infestans* act at different steps to suppress early flg22-triggered immunity. PLoS Pathog 10: e1004057. doi: 10.1371/journal.ppat.1004057 PMID: 24763622

89. Ntoukakis V, Schwessinger B, Segonzac C, Zipfel C (2011) Cautionary notes on the use of C-terminal BAK1 fusion proteins for functional studies. Plant Cell 23: 3871–3878. doi: 10.1105/tpc.111.090779 PMID: 22129600

90. He P, Shan L, Lin NC, Martin GB, Kemmerling B, Nurnberger T, et al. (2006) Specific bacterial suppressors of MAMP signaling upstream of MAPKKK in Arabidopsis innate immunity. Cell 125: 563–575. PMID: 16678099

91. Gimenez-Ibanez S, Hann DR, Ntoukakis V, Petutschnig E, Lipka V, Rathjen JP (2009) AvrPtoB targets the LysM receptor kinase CERK1 to promote bacterial virulence on plants. Curr Biol 19: 423–429. doi: 10.1016/j.cub.2009.01.054 PMID: 19249211

92. Hann DR, Rathjen JP (2007) Early events in the pathogenicity of *Pseudomonas syringae* on *Nicotiana benthamiana*. Plant J 49: 607–618. PMID: 17217460

93. Albrecht C, Boutrot F, Segonzac C, Schwessinger B, Gimenez-Ibanez S, Chinchilla D, et al. (2012) Brassinosteroids inhibit pathogen-associated molecular pattern-triggered immune signaling independent of the receptor kinase BAK1. Proc Natl Acad Sci U S A 109: 303–308. doi: 10.1073/pnas.1109921108 PMID: 22087006

94. Clough SJ, Bent AF (1998) Floral dip: a simplified method for *Agrobacterium*-mediated transformation of *Arabidopsis thaliana*. Plant J 16: 735–743. PMID: 10069079

95. Liu Y, Schiff M, Marathe R, Dinesh-Kumar SP (2002) Tobacco Rar1, EDS1 and NPR1/NIM1 like genes are required for N-mediated resistance to tobacco mosaic virus. Plant J 30: 415–429. PMID: 12028572

96. Ratcliff F, Martin-Hernandez AM, Baulcombe DC (2001) Technical Advance. Tobacco rattle virus as a vector for analysis of gene function by silencing. Plant J 25: 237–245. PMID: 11169199

97. Helliwell C, Waterhouse P (2003) Constructs and methods for high-throughput gene silencing in plants. Methods 30: 289–295. PMID: 12828942

98. Kamoun S, van der Lee T, van den Berg-Velthuis G, de Groot KE, Govers F (1998) Loss of Production of the Elicitor Protein INF1 in the Clonal Lineage US-1 of *Phytophthora infestans*. Phytopathology 88: 1315–1323. doi: 10.1094/PHYTO.1998.88.12.1315 PMID: 18944834

99. Oh SK, Young C, Lee M, Oliva R, Bozkurt TO, Cano LM, et al. (2009) In planta expression screens of *Phytophthora infestans* RXLR effectors reveal diverse phenotypes, including activation of the *Solanum bulbocastanum* disease resistance protein Rpi-blb2. Plant Cell 21: 2928–2947. doi: 10.1105/tpc.109.068247 PMID: 19794118

100. Caillaud MC, Wirthmueller L, Sklenar J, Findlay K, Piquerez SJ, Jones AM, et al. (2014) The plasmodesmal protein PDLP1 localises to haustoria-associated membranes during downy mildew infection and regulates callose deposition. PLoS Pathog 10: e1004496. doi: 10.1371/journal.ppat.1004496 PMID: 25393742

101. Edgar RC (2004) MUSCLE: multiple sequence alignment with high accuracy and high throughput. Nucleic Acids Res 32: 1792–1797. PMID: 15034147

102. Stamatakis A, Ludwig T, Meier H (2005) RAxML-III: a fast program for maximum likelihood-based inference of large phylogenetic trees. Bioinformatics 21: 456–463. PMID: 15608047

103. Team RC (2013) R: A language and environment for statistical computing. R Foundation for Statistical Computing, Vienna, Austria. URL http://www.R-project.org/.

104. Vogel F, Hofius D, Sonnewald U (2007) Intracellular trafficking of Potato leafroll virus movement protein in transgenic Arabidopsis. Traffic 8: 1205–1214. PMID: 17631001